Electronic Supplementary Material (ESI) for Journal of Materials Chemistry A.

Supplemental Information

Diffusion and selectivity of water confined within metal-organic nanotubes.

Ashini S. Jayasinghe, Maurice Payne, Daniel Unruh, Adam Johns, Johna Leddy* and Tori Z. Forbes*

Department of Chemistry, University of Iowa, Iowa City, IA 52242

* corresponding authors: johna-leddy@uiowa.edu; tori-forbes@uiowa.edu

Table of Contents

1. The Model

Consider a pore of length ℓ and radius r where $\ell/r >> 1$ so transport down the pore can be rate limiting and only one dimension x is considered along the length of the pore. Pore diagram is shown in Figure .1. Allow a gas (e.g., H_2O) to diffusion down the pore with diffusion coefficient D where $c\left(x,t\right)$ is the concentration of gas at distance x into the pore at time t. Molecules in the gas phase can condense on the pore wall. Allow condensed gas (liquid or solid) is denser than the gas, so weight in the pore will increase with time. Allow the phase change (adsorption or condensation) to occur as a first order rate, $k\left(s^{-1}\right)$. The rate water is lost from the gas phase in time and space is

$$\frac{\partial c\left(x,t\right)}{\partial t} = -kc\left(x,t\right) \tag{SI.1}$$

The rate of loss from the gas phase within the pore is the rate of condensation to the liquid phase. For no material condensed at $t = 0$ and no gas in the pore $c\left(x,0\right) = 0$, the amount condensed at time t is then expressed as accumulation down the length of the pore since the onset of condensation ($t = 0$) to time t. Given Equation 1,

$$\begin{aligned} c_{condensed}\left(t\right) &= \int_0^\ell \int_0^t kc\left(y,\omega\right)d\omega dy \quad &\text{(SI.2)} \\ &= \int_0^\ell \int_0^t dc\left(x,t\right)dy \quad &\text{(SI.3)} \\ &= \int_0^\ell \left[c\left(x,t\right) - c\left(x,0\right)\right]dy \quad &\text{(SI.4)} \\ &= \int_0^\ell c\left(y,t\right)dy \quad &\text{(SI.5)} \end{aligned}$$

A sample is composed of porous particles with N straight pores per gram of sample and surface area per one pore $SA = 2\pi r\ell$. The total weight condensed per gram of dry sample at time t is expressed as weight fraction $w\left(t\right)$.

$$\begin{aligned} w\left(t\right) &= 2\pi r\ell N \int_0^t \int_0^\ell kc\left(y,\omega\right)dy d\omega \quad &\text{(SI.6)} \\ &= 2\pi r\ell N \int_0^\ell c\left(y,t\right)dy \quad &\text{(SI.7)} \end{aligned}$$

The limits on $w\left(t\right)$ are 0 and the pore filled with water, where $w\left(t\right) - \longrightarrow N \times Vol_{1\ pore} \times \rho_{H_2O,condensed} = N\pi r^2\ell\rho_{H_2O,condensed}$. The density of water condensed in the pores $\rho_{H_2O,condensed}$ may differ from bulk water.

2. Specify the Problem

Specify the problem as a diffusion problem in one dimension. Specification is set in terms of $c\left(x,t\right)$ concentration in the gas phase (g/cm^3). The estimate is that gas is sorbed from gas phase into the pore with sufficiently large energy that sorbate does not significantly partition back into the gas phase. Gas can diffuse from both ends of the pore at $x = 0$ and $x = \ell$.

Fick's second law where D is the diffusion coefficient of the gas phase species is a loss of gas phase species at a rate k is

$$\frac{\partial c\left(x,t\right)}{\partial t} = D\frac{\partial^2 c\left(x,t\right)}{\partial x^2} - kc\left(x,t\right) \tag{SI.8}$$

This requires one initial and two boundary conditions. Let c^* be the concentration in the gas, where c^* is in grams per cm^3. The conversion of relative humidity (e.g., 60 %, 80 %...) to c^* (g/cm^3) is presented in Section 6.1.

$$\begin{aligned} c\left(x,0\right) &= 0 \quad &\text{(SI.9)} \\ c\left(0,t\right) &= c\left(\ell,t\right) = c^* \quad &\text{(SI.10)} \end{aligned}$$

The fraction of weight adsorbed is

$$w\left(t\right) = 2\pi r\ell N \int_0^\ell c\left(y,t\right)dy \tag{SI.11}$$

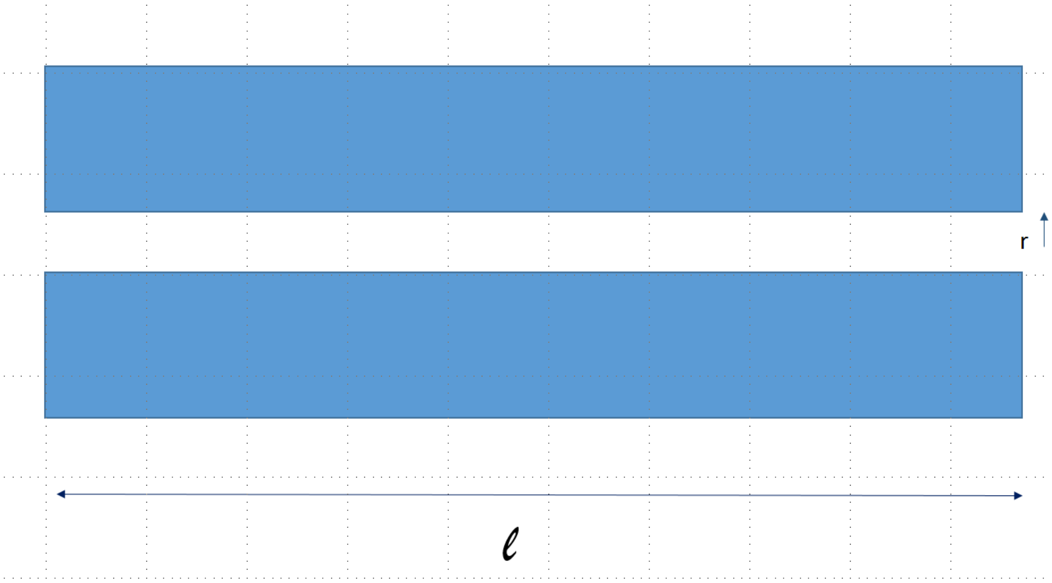

Figure SI.1: The geometry of the modeled system for pore of radious r and length of ℓ. Vapor diffuses into the pore from $x = 0$ and $x = \ell$.

3. Solution to the Problem

The specified problem is linear and solved by Laplace transform to yield an infinite series solution.

3.1 Laplace Transform (LT) of Problem

LT of Equation 8 is

$$s\bar{c}\left(x,s\right) - c\left(x,0\right) = D\frac{\partial^2 \bar{c}\left(x,s\right)}{\partial x^2} - k\bar{c}\left(x,s\right) \tag{SI.12}$$

Substitution of the initial condition, Equation 9, $c\left(x,0\right) = 0$

$$\left(s+k\right)\bar{c}\left(x,s\right) = D\frac{\partial^2 \bar{c}\left(x,s\right)}{\partial x^2} \tag{SI.13}$$

This ordinary differential equation (ODE) has a solution of the form

$$\bar{c}\left(x,s\right) = A\exp\left[-\sqrt{\frac{s+k}{D}}x\right] + B\exp\left[\sqrt{\frac{s+k}{D}}x\right] \tag{SI.14}$$

A and B are found from the two conditions in equation 10, $c\left(0,t\right) = c\left(\ell,t\right) = c^*$. On substituting the two conditions,

$$\bar{c}\left(\ell,s\right) = A\exp\left[-\sqrt{\frac{s+k}{D}}\ell\right] + B\exp\left[\sqrt{\frac{s+k}{D}}\ell\right] = \frac{c^*}{s} \tag{SI.15}$$

$$\bar{c}\left(0,s\right) = A + B = \frac{c^*}{s} \tag{SI.16}$$

On rearranging Equation 15,

$$B = \frac{c^*}{s}\exp\left[-\sqrt{\frac{s+k}{D}}\ell\right] - A\exp\left[-2\sqrt{\frac{s+k}{D}}\ell\right] \tag{SI.17}$$

On substitution of Equation 16, A and B are defined.

$$\begin{aligned}
A+B &= \frac{c^*}{s} = \frac{c^*}{s}\exp\left[-\sqrt{\frac{s+k}{D}}\ell\right] + A \quad 1-\exp\left[-2\sqrt{\frac{s+k}{D}}\ell\right]\Bigg) && \text{(SI.18)}\\
A &= \frac{c^*}{s}\frac{1-\exp\left[-\sqrt{\frac{s+k}{D}}\ell\right]}{1-\exp\left[-2\sqrt{\frac{s+k}{D}}\ell\right]} && \text{(SI.19)}\\
B &= \frac{c^*}{s}\exp\left[-\sqrt{\frac{s+k}{D}}\ell\right] - \frac{c^*}{s}\exp\left[-2\sqrt{\frac{s+k}{D}}\ell\right]\frac{1-\exp\left[-\sqrt{\frac{s+k}{D}}\ell\right]}{1-\exp\left[-2\sqrt{\frac{s+k}{D}}\ell\right]} && \text{(SI.20)}
\end{aligned}$$

Substitution of A and B into Equation 14 yields

$$\begin{aligned}
\overline{c}\left(x,s\right) &= A\exp\left[-\sqrt{\frac{s+k}{D}}x\right] + B\exp\left[\sqrt{\frac{s+k}{D}}x\right] && \text{(SI.21)}\\
&= \frac{c^*}{s}\frac{1-\exp\left[-\sqrt{\frac{s+k}{D}}\ell\right]}{1-\exp\left[-2\sqrt{\frac{s+k}{D}}\ell\right]}\exp\left[-\sqrt{\frac{s+k}{D}}x\right] + \frac{c^*}{s}\exp\left[\sqrt{\frac{s+k}{D}}x\right]\left(\begin{array}{c}\exp\left[-\sqrt{\frac{s+k}{D}}\ell\right]\\ -\exp\left[-2\sqrt{\frac{s+k}{D}}\ell\right]\frac{1-\exp\left[-\sqrt{\frac{s+k}{D}}\ell\right]}{1-\exp\left[-2\sqrt{\frac{s+k}{D}}\ell\right]}\end{array}\right)\\
\overline{c}\left(x,s\right) &= \frac{c^*}{s}\exp\left[-\sqrt{\frac{s+k}{D}}\left[\ell-x\right]\right] + \frac{c^*}{s}\left\{\begin{array}{c}\dfrac{\begin{array}{c}\exp\left[-\sqrt{\frac{s+k}{D}}x\right]-\exp\left[-\sqrt{\frac{s+k}{D}}\left[\ell+x\right]\right]\\ -\exp\left[-\sqrt{\frac{s+k}{D}}\left[2\ell-x\right]\right]+\exp\left[-\sqrt{\frac{s+k}{D}}\left[3\ell-x\right]\right]\end{array}}{1-\exp\left[-2\sqrt{\frac{s+k}{D}}\ell\right]}\\ \\ \end{array}\right\} && \text{(SI.22)}
\end{aligned}$$

For $ax<1$, $\frac{1}{1-e^{ax}} = 1+e^{ax}+e^{2ax}+.... = \sum_{j=0} e^{jax}$. Equation 22 is expressed as a series.

$$\begin{aligned}
\overline{c}\left(x,s\right) &= \frac{c^*}{s}\exp\left[-\sqrt{\frac{s+k}{D}}\left[\ell-x\right]\right] && \text{(SI.23)}\\
&+\frac{c^*}{s}\left\{\begin{array}{c}\exp\left[-\sqrt{\frac{s+k}{D}}x\right]-\exp\left[-\sqrt{\frac{s+k}{D}}\left[\ell+x\right]\right]\\ -\exp\left[-\sqrt{\frac{s+k}{D}}\left[2\ell-x\right]\right]+\exp\left[-\sqrt{\frac{s+k}{D}}\left[3\ell-x\right]\right]\end{array}\right\}\sum_{j=0}\exp\left[-2j\ell\sqrt{\frac{s+k}{D}}\right]\\
\overline{c}\left(x,s\right) &= \frac{c^*}{s}\exp\left[-\sqrt{\frac{s+k}{D}}\left[\ell-x\right]\right] + \frac{c^*}{s}\sum_{j=0}\exp\left[-\left[2j\ell+x\right]\sqrt{\frac{s+k}{D}}\right] && \text{(SI.24)}\\
&-\frac{c^*}{s}\sum_{j=0}\exp\left[-\left[\left(2j+1\right)\ell+x\right]\sqrt{\frac{s+k}{D}}\right] - \frac{c^*}{s}\sum_{j=0}\exp\left[-\left[2\left(j+1\right)\ell-x\right]\sqrt{\frac{s+k}{D}}\right]\\
&+\frac{c^*}{s}\sum_{j=0}\exp\left[-\left[\left(2j+3\right)\ell-x\right]\sqrt{\frac{s+k}{D}}\right]
\end{aligned}$$

The problem is solved for $c\left(x,t\right)$ by finding the inverse Laplace transform of Equation 24.

3.2 Inverse Laplace Transform of $c\left(x,s\right)$ Derives $c\left(x,t\right)$

This expression for $c\left(x,s\right)$ is complex and might be simplified in various ways, but the inverse Laplace transform is readily specified. From Doestch [1], where $\operatorname{erf} c\left(z\right)$ is the error function complement[1] of z,

$$\frac{\exp\left[-\alpha\sqrt{s+k}\right]}{s} \Leftrightarrow \frac{1}{2}\left[\exp\left[-\alpha\sqrt{k}\right]\operatorname{erf} c\left[\frac{\alpha}{2\sqrt{t}}-\sqrt{kt}\right]+\exp\left[\alpha\sqrt{k}\right]\operatorname{erf} c\left[\frac{\alpha}{2\sqrt{t}}+\sqrt{kt}\right]\right] \tag{SI.26}$$

Then, the termwise inverse for Equation 24 yields $c\left(x,t\right)$.

$$\frac{2c\left(x,t\right)}{c^{*}} = \left[\begin{array}{c} \exp\left[-\left(\ell-x\right)\sqrt{\frac{k}{D}}\right]\operatorname{erf} c\left[\frac{\ell-x}{2\sqrt{Dt}}-\sqrt{kt}\right] \\ +\exp\left[\left(\ell-x\right)\sqrt{\frac{k}{D}}\right]\operatorname{erf} c\left[\frac{\ell-x}{2\sqrt{Dt}}+\sqrt{kt}\right] \end{array}\right] \tag{SI.27}$$

$$+\sum_{j=0}\left[\begin{array}{c} \exp\left[-\left(2j\ell+x\right)\sqrt{\frac{k}{D}}\right]\operatorname{erf} c\left[\frac{2j\ell+x}{2\sqrt{Dt}}-\sqrt{kt}\right] \\ +\exp\left[\left(2j\ell+x\right)\sqrt{\frac{k}{D}}\right]\operatorname{erf} c\left[\frac{2j\ell+x}{2\sqrt{Dt}}+\sqrt{kt}\right] \end{array}\right] \tag{SI.28}$$

$$-\sum_{j=0}\left[\begin{array}{c} \exp\left[-\left(\left(2j+1\right)\ell+x\right)\sqrt{\frac{k}{D}}\right]\operatorname{erf} c\left[\frac{\left(2j+1\right)\ell+x}{2\sqrt{Dt}}-\sqrt{kt}\right] \\ +\exp\left[\left(\left(2j+1\right)\ell+x\right)\sqrt{\frac{k}{D}}\right]\operatorname{erf} c\left[\frac{\left(2j+1\right)\ell+x}{2\sqrt{Dt}}+\sqrt{kt}\right] \end{array}\right]$$

$$-\sum_{j=0}\left[\begin{array}{c} \exp\left[-\left(2\left(j+1\right)\ell-x\right)\sqrt{\frac{k}{D}}\right]\operatorname{erf} c\left[\frac{2\left(j+1\right)\ell-x}{2\sqrt{Dt}}-\sqrt{kt}\right] \\ +\exp\left[\left(2\left(j+1\right)\ell-x\right)\sqrt{\frac{k}{D}}\right]\operatorname{erf} c\left[\frac{2\left(j+1\right)\ell-x}{2\sqrt{Dt}}+\sqrt{kt}\right] \end{array}\right]$$

$$+\sum_{j=0}\left[\begin{array}{c} \exp\left[-\left(\left(2j+3\right)\ell-x\right)\sqrt{\frac{k}{D}}\right]\operatorname{erf} c\left[\frac{\left(2j+3\right)\ell-x}{2\sqrt{Dt}}-\sqrt{kt}\right] \\ +\exp\left[\left(\left(2j+3\right)\ell-x\right)\sqrt{\frac{k}{D}}\right]\operatorname{erf} c\left[\frac{\left(2j+3\right)\ell-x}{2\sqrt{Dt}}+\sqrt{kt}\right] \end{array}\right]$$

3.3 Limiting Behavior of $c\left(x,t\right)$

The behavior at early and late time can be considered. A limiting response for $c\left(x,t\right)$ at early or late times allows ready determination of parameters from the weight data. The initial and final value theorems allow evaluation of limits as $t\longrightarrow 0$ and $t\longrightarrow\infty$. Initial and final value theorems are applied to $c\left(x,s\right)$.

3.3.1 Early Time Behavior of $c\left(x,t\right)$

The initial value limit theorem

$$\lim_{t\longrightarrow 0} f\left(t\right) = \lim_{s\longrightarrow\infty} sF\left(s\right) \tag{SI.29}$$

---

[1] The error function characterizes the area under the probability distribution from 0 to z.

$$\operatorname{erf} z = \frac{2}{\sqrt{\pi}}\int_{0}^{z} e^{-x^{2}}\,dx \tag{SI.25}$$

The properties of the error function are

$$\begin{array}{rcl} \operatorname{erf}\left(-z\right) & = & -\operatorname{erf}\left(z\right) \\ \operatorname{erf}\left(z\right)+\operatorname{erf} c\left(z\right) & = & 1 \\ \operatorname{erf} c\left(z\right) & = & 1-\operatorname{erf}\left(z\right) \\ \operatorname{erf} c\left(-z\right) & = & 1-\operatorname{erf}\left(-z\right)=1+\operatorname{erf}\left(z\right) \\ \lim\limits_{z\longrightarrow\infty}\operatorname{erf} c\left(z\right) & \longrightarrow & 0 \\ \lim\limits_{z\longrightarrow\infty}\operatorname{erf} c\left(-z\right) & = & \lim\limits_{z\longrightarrow\infty}\left(1+\operatorname{erf}\left(z\right)\right)\longrightarrow 2 \end{array}$$

is applied to Equation 23 to yield the early time response.

$$\begin{aligned}\lim_{t\longrightarrow 0} c\left(x,t\right) &= \lim_{s\longrightarrow\infty} sc\left(x,s\right) \qquad \text{(SI.30)}\\ &= \lim_{s\longrightarrow\infty} s\left\{\begin{array}{c}\frac{c^*}{s}\exp\left[-\sqrt{\frac{s+k}{D}}\left[\ell-x\right]\right]\\ +\frac{c^*}{s}\left\{\begin{array}{c}\exp\left[-\sqrt{\frac{s+k}{D}}x\right]-\exp\left[-\sqrt{\frac{s+k}{D}}\left[\ell+x\right]\right]\\ -\exp\left[-\sqrt{\frac{s+k}{D}}\left[2\ell-x\right]\right]+\exp\left[-\sqrt{\frac{s+k}{D}}\left[3\ell-x\right]\right]\end{array}\right\}\sum_{j=0}\exp\left[-2j\ell\sqrt{\frac{s+k}{D}}\right]\end{array}\right\}\\ &\longrightarrow 0\end{aligned}$$

This yields the initial condition that there is no solvent in the pore at the start of the experiment, consistent with Equation 9. This outcome serves as check of the derivation but does not provide access to model parameters.

3.3.2 Late Time, Time Invariant Behavior of $c\left(x,t\right)$

The final value theorem is similar to the initial value theorem.

$$\lim_{t\longrightarrow\infty} f\left(t\right) = \lim_{s\longrightarrow 0} sF\left(s\right) \qquad \text{(SI.31)}$$

Application of the final value theorem to Equation 24 yields the final concentration.

$$\begin{aligned}\lim_{t\longrightarrow\infty} c\left(x,t\right) &= \lim_{s\longrightarrow 0} sc\left(x,s\right) \qquad \text{(SI.32)}\\ &= \lim_{s\longrightarrow 0} s\left\{\begin{array}{c}\frac{c^*}{s}\exp\left[-\sqrt{\frac{s+k}{D}}\left[\ell-x\right]\right]\\ +\frac{c^*}{s}\left\{\begin{array}{c}\exp\left[-\sqrt{\frac{s+k}{D}}x\right]-\exp\left[-\sqrt{\frac{s+k}{D}}\left[\ell+x\right]\right]\\ -\exp\left[-\sqrt{\frac{s+k}{D}}\left[2\ell-x\right]\right]+\exp\left[-\sqrt{\frac{s+k}{D}}\left[3\ell-x\right]\right]\end{array}\right\}\sum_{j=0}\exp\left[-2j\ell\sqrt{\frac{s+k}{D}}\right]\end{array}\right\}\\ &\longrightarrow c^*\exp\left[-\sqrt{\frac{k}{D}}\left[\ell-x\right]\right]+c^*\left\{\begin{array}{c}\exp\left[-\sqrt{\frac{k}{D}}x\right]-\exp\left[-\sqrt{\frac{k}{D}}\left[\ell+x\right]\right]\\ -\exp\left[-\sqrt{\frac{k}{D}}\left[2\ell-x\right]\right]+\exp\left[-\sqrt{\frac{k}{D}}\left[3\ell-x\right]\right]\end{array}\right\}\sum_{j=0}\exp\left[-2j\ell\sqrt{\frac{k}{D}}\right]\\ &= c^*\exp\left[-\sqrt{\frac{k}{D}}\left[\ell-x\right]\right]+c^*\frac{\exp\left[-\sqrt{\frac{k}{D}}x\right]\left(1-\exp\left[-\ell\sqrt{\frac{k}{D}}\right]\right)}{1-\exp\left[-2\ell\sqrt{\frac{k}{D}}\right]}\\ &\quad -c^*\frac{\exp\left[\sqrt{\frac{k}{D}}x\right]\exp\left[-\sqrt{\frac{k}{D}}2\ell\right]\left(1-\exp\left[-\ell\sqrt{\frac{k}{D}}\right]\right)}{1-\exp\left[-2\ell\sqrt{\frac{k}{D}}\right]}\\ &= c^*\exp\left[-\sqrt{\frac{k}{D}}\left[\ell-x\right]\right]+c^*\frac{1-\exp\left[-\ell\sqrt{\frac{k}{D}}\right]}{1-\exp\left[-2\ell\sqrt{\frac{k}{D}}\right]}\left[\exp\left[-\sqrt{\frac{k}{D}}x\right]-\exp\left[\sqrt{\frac{k}{D}}x\right]\exp\left[-\sqrt{\frac{k}{D}}2\ell\right]\right]\end{aligned}$$

After additional algebraic steps, the final value of $\lim_{t\longrightarrow\infty} c\left(x,t\right)$ is found.

$$\lim_{t\longrightarrow\infty} c\left(x,t\right) = c\left(x,\infty\right) = c^*\frac{1}{1+\exp\left[-\ell\sqrt{\frac{k}{D}}\right]}\left\{\exp\left[\sqrt{\frac{k}{D}}x\right]\exp\left[-\sqrt{\frac{k}{D}}\ell\right]+\exp\left[-\sqrt{\frac{k}{D}}x\right]\right\} \qquad \text{(SI.33)}$$

Equation 33 is consistent with the boundary conditions and serves to check the derivation. At $x=0$, $c\left(0,t\right)=c^*$ and at $x=\ell$, $c\left(\ell,t\right)=c^*$, consistent with Equations 10.

Equation 33 allows calculation of the final, time invariant weight condensed into the pore, w_{eq}, where w_{eq} is the equilibrium weight fraction in the pore.

3.4 Introduction of Dimensionless Variables

Dimensionless variables allow more facile comparison of competing phenomena, such as rate of transport and rate of condensation. Dimensionless variables also facilitate fitting model equations to data. Consider several dimensionless parameters. A dimensionless ratio of time t to rate of condensation $k\ \left(s^{-1}\right)$ is defined by τ where

$$\tau = \sqrt{kt} \tag{SI.34}$$

$$\tau^2 = kt \tag{SI.35}$$

A dimensionless ratio of reaction rate to transport is described by β where

$$\beta = \frac{\ell\sqrt{k}}{\sqrt{D}} \tag{SI.36}$$

As reaction rate increases relative to transport in the pore, β increases. A alternative dimensionless time is defined by ratio of β to τ.

$$\frac{\beta}{\tau} = \frac{\ell}{\sqrt{Dt}} \tag{SI.37}$$

These parameters will allow characterization of $w\left(t\right)$.

For completeness, a dimensionless distance $p = \frac{x}{\ell}$ is introduced. The dimensionless concentration is defined as

$$f\left(x,t\right) = \frac{c\left(x,t\right)}{c^*} \tag{SI.38}$$

where c^* is the concentration of the gas in the matrix outside pores (g/cm^2).

Introduction of dimensionless parameters into Equation 27 yields the dimensionless fractional concentration.

$$\begin{aligned} 2f\left(x,t\right) = & \left[\begin{array}{l} \exp\left[-\left(1-p\right)\beta\right]\mathrm{erf}\,c\left[\frac{1-p}{2}\frac{\beta}{\tau}-\tau\right] \\ +\exp\left[\left(1-p\right)\beta\right]\mathrm{erf}\,c\left[\frac{1-p}{2}\frac{\beta}{\tau}+\tau\right] \end{array}\right] + \sum_{j=0}\left[\begin{array}{l} \exp\left[-\left(2j+p\right)\beta\right]\mathrm{erf}\,c\left[\frac{(2j+p)}{2}\frac{\beta}{\tau}-\tau\right] \\ +\exp\left[\left(2j+p\right)\beta\right]\mathrm{erf}\,c\left[\frac{(2j+p)}{2}\frac{\beta}{\tau}+\tau\right] \end{array}\right] \\ & -\sum_{j=0}\left[\begin{array}{l} \exp\left[-\left(\left(2j+1\right)+p\right)\beta\right]\mathrm{erf}\,c\left[\frac{(2j+1)+p}{2}\frac{\beta}{\tau}-\tau\right] \\ +\exp\left[\left(\left(2j+1\right)+p\right)\beta\right]\mathrm{erf}\,c\left[\frac{(2j+1)+p}{2}\frac{\beta}{\tau}+\tau\right] \end{array}\right] \\ & -\sum_{j=0}\left[\begin{array}{l} \exp\left[-\left(2\left(j+1\right)-p\right)\beta\right]\mathrm{erf}\,c\left[\frac{2(j+1)-p}{2}\frac{\beta}{\tau}-\tau\right] \\ +\exp\left[\left(2\left(j+1\right)-p\right)\beta\right]\mathrm{erf}\,c\left[\frac{2(j+1)-p}{2}\frac{\beta}{\tau}+\tau\right] \end{array}\right] \\ & +\sum_{j=0}\left[\begin{array}{l} \exp\left[-\left(\left(2j+3\right)-p\right)\beta\right]\mathrm{erf}\,c\left[\frac{(2j+3)-p}{2}\frac{\beta}{\tau}-\tau\right] \\ +\exp\left[\left(\left(2j+3\right)-p\right)\beta\right]\mathrm{erf}\,c\left[\frac{(2j+3)-p}{2}\frac{\beta}{\tau}+\tau\right] \end{array}\right] \end{aligned} \tag{SI.39}$$

4 Weight $w\left(t\right)$

The weight fraction in the pore, $w\left(t\right)$ is defined by the amount condensed at time t. Integration of the concentration at time t down the length of the pore yields $w\left(t\right)$ by Equation 11.

$$w\left(t\right) = 2\pi r\ell N\int_0^\ell c\left(y,t\right)dy = 2\pi r\ell Nc^*\int_0^\ell f\left(y,t\right)dy \tag{SI.40}$$

4.1 Equilibrium Weight Fraction w_{eq}

The equilibrium weight fraction in the pore, w_{eq} is analogously dependent on integration of $c\left(x,\infty\right)$ as defined in Equation 33.

$$w_{eq} = 2\pi r\ell N \int_0^{\ell} c\left(y,\infty\right)dy \tag{SI.41}$$

where

$$\begin{aligned}
\int_0^{\ell} c\left(x,\infty\right)dx &= c^* \frac{1}{1+\exp\left[-\ell\sqrt{\frac{k}{D}}\right]} \int_0^{\ell} \left\{\exp\left[\sqrt{\frac{k}{D}}x\right]\exp\left[-\sqrt{\frac{k}{D}}\ell\right] + \exp\left[-\sqrt{\frac{k}{D}}x\right]\right\}dx \qquad \text{(SI.42)} \\
&= c^* \frac{1}{1+\exp\left[-\ell\sqrt{\frac{k}{D}}\right]} \left\{\begin{array}{c} \sqrt{\frac{D}{k}}\exp\left[\sqrt{\frac{k}{D}}x\right]\exp\left[-\sqrt{\frac{k}{D}}\ell\right] \\ +\left(-\sqrt{\frac{D}{k}}\right)\exp\left[-\sqrt{\frac{k}{D}}x\right] \end{array}\right\}\Bigg|_0^{\ell} \\
&= 2\sqrt{\frac{D}{k}}c^* \frac{1-\exp\left[-\sqrt{\frac{k}{D}}\ell\right]}{1+\exp\left[-\ell\sqrt{\frac{k}{D}}\right]} = 2\sqrt{\frac{D}{k}}c^* \frac{\exp\left[\frac{\ell}{2}\sqrt{\frac{k}{D}}\right]-\exp\left[-\frac{\ell}{2}\sqrt{\frac{k}{D}}\right]}{\exp\left[+\frac{\ell}{2}\sqrt{\frac{k}{D}}\right]+\exp\left[-\frac{\ell}{2}\sqrt{\frac{k}{D}}\right]} \\
\int_0^{\ell} c\left(x,\infty\right)dx &= 2c^*\sqrt{\frac{D}{k}}\tanh\left[\frac{\ell}{2}\sqrt{\frac{k}{D}}\right] \qquad \text{(SI.43)}
\end{aligned}$$

Or dimensionlessly,

$$\int_0^{\ell} \frac{c\left(x,\infty\right)}{c^*}dx = \int_0^{\ell} f\left(x,\infty\right)dx = 2\sqrt{\frac{D}{k}}\tanh\left[\frac{\beta}{2}\right] = 2\frac{\ell}{\beta}\tanh\left[\frac{\beta}{2}\right] \tag{SI.44}$$

and

$$\begin{aligned}
w_{eq} &= w\left(t\longrightarrow\infty\right) = 2\pi r\ell Nc^* \int_0^{\ell} f\left(y,\infty\right)dy \qquad \text{(SI.45)} \\
w_{eq} &= 4\pi r\ell^2 Nc^* \frac{1}{\beta}\tanh\left[\frac{\beta}{2}\right] = 4\pi r\ell Nc^* \sqrt{D/k}\tanh\left[\frac{\beta}{2}\right] \qquad \text{(SI.46)}
\end{aligned}$$

When the equilibrium weight w_{eq} is found experimentally, w_{eq} provides access to significant characterization parameters. A few items of note arise from Equation SI.46.

1. Note that both w_{eq} and $4\pi r\ell^2 Nc^*$ are dimensionless.
2. Several constraints accrue from the $\tanh\left[\beta/2\right]$.
   (a) For $\beta = \ell\sqrt{k/D} > 10$, $\tanh(\beta/2) \longrightarrow 1$ and $w_{eq} = 4\pi r\ell Nc^*\sqrt{D/k}$. $\beta > 10$ corresponds to fast reaction rate compared to mass transport, D/ℓ^2.
   (b) For $\beta \lesssim 0.25$, $\tanh\left(\beta/2\right) \longrightarrow \beta/2$ and $w_{eq} = 2\pi r\ell^2 Nc^*$. This corresponds to small k and little condensation, so w_{eq} is just the mass of gas in the pores. It is probable this is too little mass to measure experimentally.
3. Typically, the time scale to complete a diffusion processes is roughly $Dt/\ell^2 = \left[\tau/\beta\right]^2 \lesssim 5$.

4.2 Expressions Used to Generate Fitting of $w\left(t\right)$

The solution to the specified problem is analytic but requires evaluation of several infinite sums. To do so, the summations are evaluated in a spreadsheet (Excel®) based on input β. Summations for values of β between 50 and 0.001 are evaluated. This range of β values covers the transition from k so large there is little to no gas in the pore at equilibrium because condensation happens rapidly to k so small there is only gas in the pore at equilibrium.

From Equation 40, $w\left(t\right) = 2\pi r\ell Nc^* \int_0^{\ell} f\left(y,t\right)dy$. Expression for $w\left(t\right)$ depend on representation of $\int_0^{\ell} f\left(y,t\right)dy$ as summations of $f\left(x,t\right)$, defined in Equation 39.

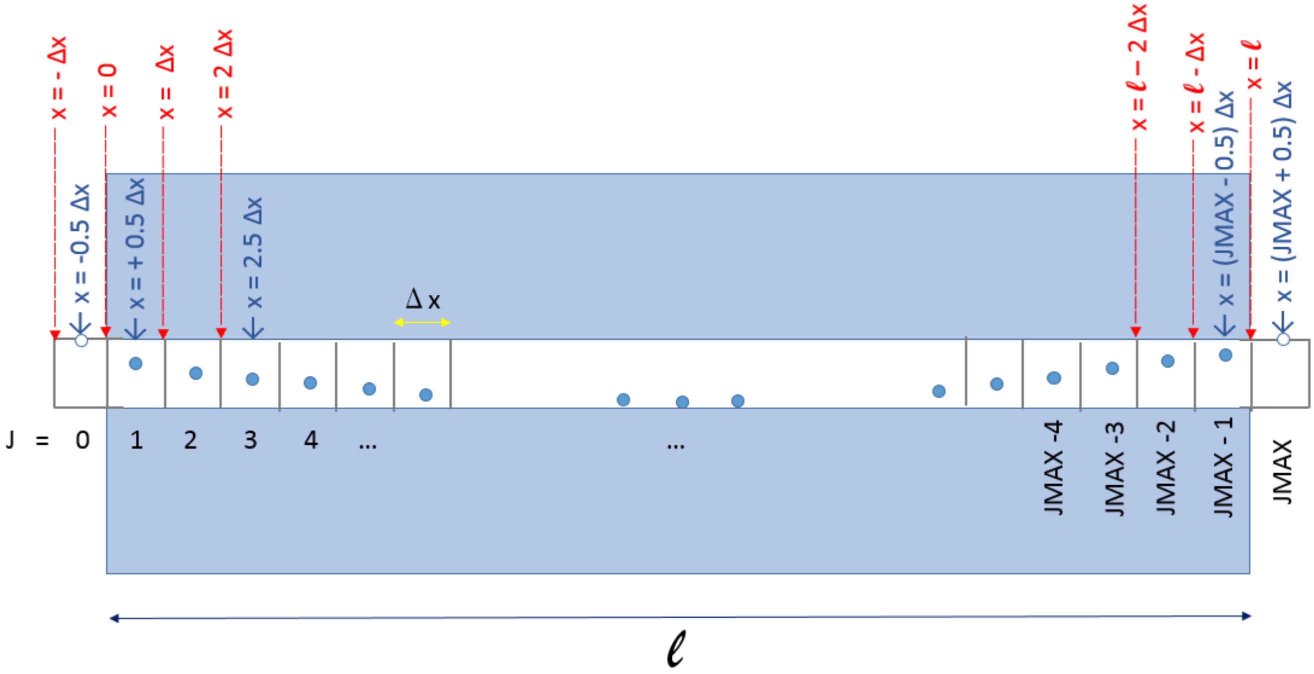

Figure SI.2: The pore is of $\ell = (JMAX - 1)\,\Delta x$. The concentration is measured at the middle of each box, as represented by the circles, so that the concentration in box $J = 1$ is measured at $x = 0.5\Delta x$ with the gas pore interface at $x = 0$ and the right edge of box $J = 1$ at $x = 1\Delta x$. At $J = 0$ and $J = JMAX$, the concentration reflects the gas phase concentration and is pinned at a value pinned by relative humidity or dimensionlessly at 1. To evaluate the total concentration in the pore, the concentrations in the middle of boxes $J = 1$ to $J = JMAX - 1$ are summed.

The objective is to evaluate $f(x,t)$ for a given t at multiple locations x down the pore ($0 \leq x \leq \ell$). Then, all values of $f(x,t)$ for the specified time are summed down the length of the pore (across x) to evaluate $\int_0^\ell f(y,t)\,dy$. This requires specifying a time and space grid with indexes of J and K, respectively. The maximum number of space elements is $JMAX$. See Figure .2. Allow a space increment Δx. Let outer edges of the pore be at $x=0$ and $x=\ell$ or at $J=\frac{1}{2}\Delta x$ and $J=\left(JMAX-\frac{1}{2}\right)\Delta x$. Then for a pore of length ℓ,

$$\Delta x = \frac{\ell}{\left(JMAX-\frac{1}{2}\right)-\frac{1}{2}} = \frac{\ell}{JMAX-1} \tag{SI.47}$$

The concentration for each position J is measured in the middle of box J, at $x_j = \{0.5, 1.5, 2.5......\ (JMAX-2.5),$ $(JMAX-1.5)$, $(JMAX-0.5)\}\Delta x$. To sum across all the boxes contained inside the pore of length ℓ, the summation is from $J=1$ to $J=JMAX-1$. Just outside the pore where $x=0$ and $x=\ell$, the concentration is pinned by the gas phase concentration set by RH, relative humidity. At $J=0$ and $J=JMAX$, the fractional concentrations are pinned at 1 in the middle of boxes where $x=-0.5\Delta x$ and $x=(JMAX+0.5)\,\Delta x$, just outside the pore, so these concentrations are not included in the sum. The larger $JMAX$, the better the resolution of the calculation because the size and so uncertainty of Δx decreases. Here, $JMAX=25$, which allows calculation with better resolution than anticipated experimental results.

The maximum number of time values to evaluate is set by $KMAX$. Here, $KMAX=20$. The choice of $KMAX$ and how the time values are selected does not impact the quality of the calculation. Here, for $0.001 \leq \beta \leq 50$, it was noted empirically that equilibrium is reached (constant w_{eq}) provided the maximum time is represented by $\tau_{\max}^2=\beta^2$, that is $\ell/\sqrt{D\tau_{\max}}=1$. Based on $KMAX$, the values of K were incremented as $K\left(\tau_{\max}/KMAX\right)$ so the calculated times are $kt=\left[K\tau_{\max}/KMAX\right]^2$. The time to equilibrium measured as τ^2 decreased as β decreased.

For each time $\tau^2=kt$ at the corresponding K, the simulation calculates $f(J,K)$ for each J according to Equation 39. The spreadsheet then calculates $sumf\left(\tau^2\right)=(JMAX-1)^{-1}\sum_{j=1}^{j\max-1} f(J,K)$

$$\begin{aligned}\sum_{j=1}^{j\max-1} f(J,K)\,\Delta x &= \frac{\ell}{JMAX-1}\sum_{j=1}^{j\max-1} f(J,K) \\ &= \ell \times sumf\left(\tau^2\right) \\ &\longrightarrow \int_0^\ell f(y,t)\,dy\end{aligned} \tag{SI.48}$$

Weight fraction $w(t)$ is defined with respect to the summation on substitution into Equation 40.

$$\begin{aligned}w(t) &= 2\pi r\ell Nc^*\int_0^\ell f(y,t)\,dy \\ &= 2\pi r\ell Nc^*\frac{\ell}{JMAX-1}\sum_{j=1}^{j\max-1} f(J,K)\end{aligned} \tag{SI.49}$$

$$w(t) = 2\pi r\ell Nc^*\ell \times sumf\left(\tau^2\right) \tag{SI.50}$$

$$= 2\frac{\varepsilon}{r}c^*\ell \times sumf(kt) \tag{SI.51}$$

Equation 51 introduces the particle porosity, $\varepsilon = N\pi r^2\ell$ where N is the number of straight pores per gram of sample, so ε has units of volume per gram of sample (cm^3/g) and $\varepsilon c^*\ell/r$ is dimensionless.

This parameterization is used in a spreadsheet to generate model curves that fit the experimental data.

5 Model Curves for $f(x,t)$ and $sumf(kt)$

The spreadsheet evaluation of $sumf\left(\tau^2\right)$ yields maps of $f(x,t)$ the fractional concentration of the gas in the pore for various inputs of β at times $\tau^2=kt$. The summation of $f(x,t)$ between 1 and $JMAX-\ 1$ yields $sumf\left(\tau^2\right)$ that maps normalized weight fraction $w(t)/\left[2\varepsilon c^*\ell/r\right]$ as a function of τ^2 or equivalently $\log[kt]$. Here outputs of fractional concentration of gas in the pore as a function of $0 \leq x \leq \ell$ with t and β characterize the interplay between diffusion in the pore and rate of condensation as well as the approach to equilibrium for the gas in the pore. Also shown are variation in $sumf\left(\tau^2\right)$ with $\log[kt]$ as a function of β, which characterizes how weight of condensed material builds in the pore over time $\tau^2 = kt$.

5.1 Equilibrium Behavior of Gas in the Pore $f(x,t)$ with $0 \leq x \leq \ell$ as a Function of β

At equilibrium, the concentration of gas in the pore is set by $\beta = \ell\sqrt{k/D}$. Consider, for example, a fixed ℓ. As the rate of condensation k increases relative to D, transport rate in the pore, the fraction of water condensed relative to the gas phase will increase. For high β, water will condense rapidly with gas concentration high near the ends of the pore and lower toward the middle. The fraction in the gas phase is $f(x,t)$.

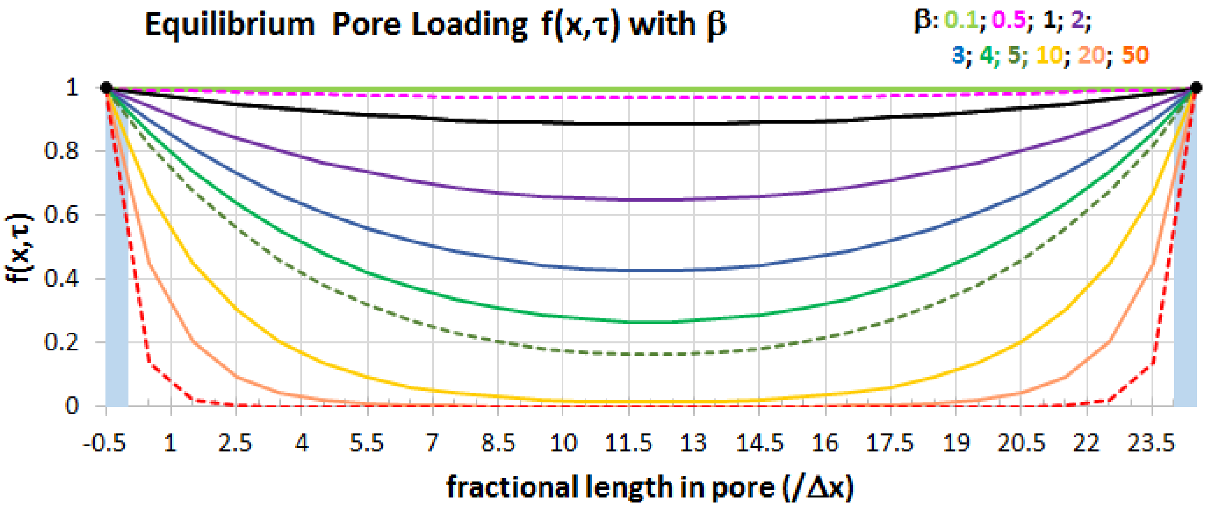

Figure SI.3: At equilibrium, $f\left(x,\tau_{eq}^2\right)$ is shown for values of β between 0.1 and 50. At $\beta \leq 0.1$, $f\left(x,\tau_{eq}^2\right) \longrightarrow 1$ for all x and the pore is fully loaded with gas, consistent with small β and the rate of condensation is low. Whne β is high, condensation is rapid and the little gas penetrates the pore only a short distance and $f\left(\ell/2,\tau_{eq}^2\right) \longrightarrow 0$ in the middle of the pore. The black line for $\beta = 1$ maps $f\left(\ell/2,\tau_{eq}^2\right)$ of 0.9.

The model (Section 1) describes the fractional weight increase dependent on condensation from the gas phase. If the condensation is rapid compared to transport (high β), little gas phase material is available to further condense and the weight condensed will be small. At equilibrium, the fractional weight of water condensed in the pore is w_{eq}. This is reflected at equilibrium in Equation 46, $w_{eq}\left[2\pi r\ell^2 Nc^*\right]^{-1} = \frac{2}{\beta}\tanh\left[\frac{\beta}{2}\right]$; when β is large, $\tanh[\beta/2] \longrightarrow 1$ and $w_{eq}\left[2\pi r\ell^2 Nc^*\right]^{-1} \longrightarrow \frac{2}{\beta}$ and w_{eq} is small. From Figure .3, $f\left(x,\tau_{eq}^2\right)$ is small across all x for large β, so w_{eq} is small.

Equation 46, $w_{eq}\left[2\pi r\ell^2 Nc^*\right]^{-1} = \frac{2}{\beta}\tanh\left[\frac{\beta}{2}\right]$ yields a plot of $w_{eq}\left[2\pi r\ell^2 Nc^*\right]^{-1}$ as a function of β, shown in Figure .4. The decrease in $w_{eq}\left[2\pi r\ell^2 Nc^*\right]^{-1}$ with increase in β reflects the limited gas phase concentration and so limited condensed weight. If $w_{eq}\left[2\pi r\ell^2 Nc^*\right]^{-1}$ is known experimentally, β can be estimated from the plot. For $\beta \lesssim 0.3$. $w_{eq}\left[2\pi r\ell^2 Nc^*\right]^{-1} \gtrsim 0.99$.

The open circles are the equilibrium weights evaluated by the spreadsheet. The equilibrium weights are well matched for $\beta < 10$. Regression of $y =$ spreadsheet $w_{eq}\left[2\pi r\ell^2 Nc^*\right]^{-1}$ with $x = \frac{2}{\beta}\tanh\left[\frac{\beta}{2}\right]$ yields slope $= (1.034 \pm 0.001)$ and intercept $= (\quad 0.035 \pm 0.001)$ for $R^2 = 0.99997$. The resolution of the simulation at $JMAX = 25$ is good for $\beta \lesssim 5$ where spreadsheet and analytic expression match within 5%; At higher β, the equilibrium values are better fit by Equation 46. In general, the spreadsheet results are reliable for
$\lesssim 5$.

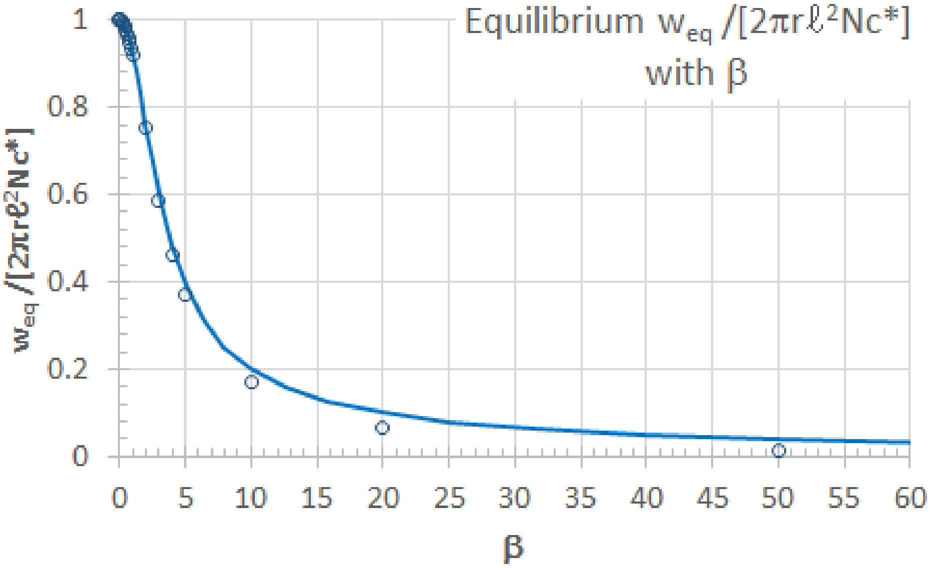

Figure SI.4: From Equation 46, $w_{eq}\left[2\pi r\ell^2Nc^*\right]^{-1} = \frac{2}{\beta}\tanh\left[\frac{\beta}{2}\right]$, a plot of $w_{eq}\left[2\pi r\ell^2Nc^*\right]^{-1}$ with β is shown as a solid line. For $\beta \lesssim 0.3$, $w_{eq}\left[2\pi r\ell^2Nc^*\right]^{-1}$ 0.99. Given $w_{eq}\left[2\pi r\ell^2Nc^*\right]^{-1}$, β is estimated from the plot. The open circles are the equilibrium values of $w_{eq}\left[2\pi r\ell^2Nc^*\right]^{-1}$ evaluated in the spreadsheet.

5.2 Time Dependent Behavior of Gas in the Pore $f(x,t)$ with $0 \le x \le \ell$ as a Function of β

The time evolution that maps the building of gas in the pore is shown for $\beta = 1$ in Figure .5 as a function of $\tau^2 = kt$. At early times, the pore is filling from the ends of the pore at $x = 0$ and $x = \ell$, and no gas phase material has reached the center of the pore. As time progresses, gas moves toward the middle of the pore and concentration builds along x until equilibrium is reached. For $\beta = 1$, the rate of condensation and the rate of transport down the pore are comparable.

For comparison, plots are shown for $\beta = 5$ and $\beta = 0.2$. For $\beta = 5$ in Figure .6, the rate of condensation is higher than the rate of transport down the pore, so there is less material at equilibrium in the pore and notably at equilibrium,as compared to $\beta = 1$ shown in Figure .5. The result is reversed for $\beta = 0.2$ shown in Figure .7, where transport down the pore is more efficient than the rate of condensation so that as compared to $\beta = 1$, the pore is completely filled with gas by the time equilibrium is reached.

The greater the fraction of gas in the pore, the greater the condensation in the pore and so the higher the measured weight.

The model yields the time evolution of weight as $sumf\left(\tau^2\right)$ versus $\log kt$ dependent on β. The variation is mapped in Figure .8.

6 Approach to Fit Experimental Data

Experimental data are available as the dimensionless $w(t)$, the weight condensed/dry weight of sample. Several notes are provided to aid in fitting the data. The fit assumes the equilibrium weight w_{eq} is measured.

6.1 Information that may be useful in fitting experimental data

Information that may be useful in fitting data are outlined. This includes calculation of c^* from relative humidity. The fitting protocol follows.

1. The concentration of the water in the gas phase c^* has units of grams gas species / cm^3, which is calculated from the percent relative humidity, RH. RH is the ratio of the mass or density in the gas phase to the maximum

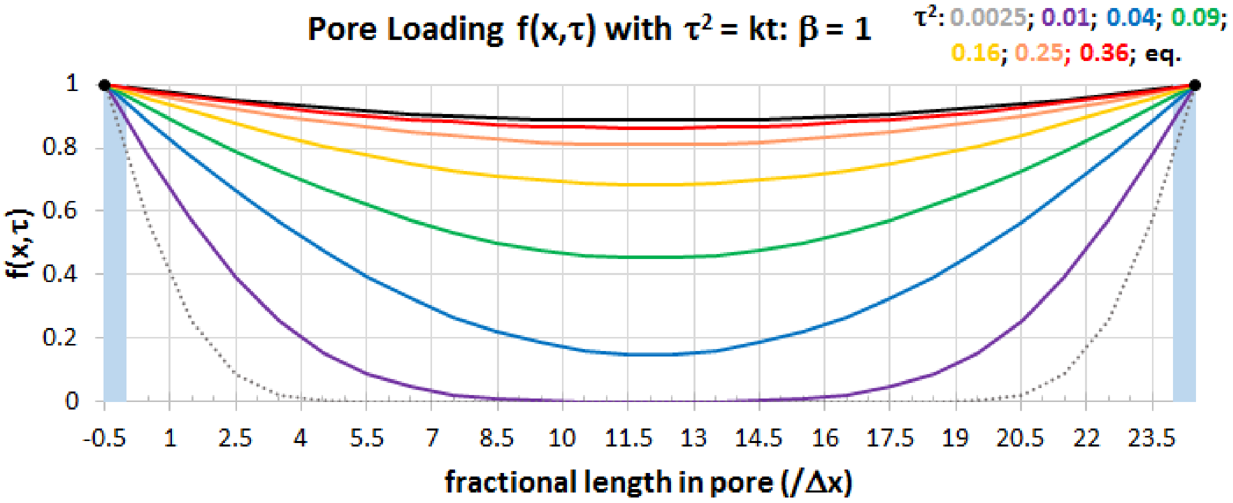

Figure SI.5: The concentration down the length of the pore is shown to increase as a function of time τ^2 where τ^2 is 0.0025, 0.01, 0.04, 0.09, 0.16, 0.25, 0.36, and equilibrium. For $\beta = 1$, at equilirbrium the pore is filled $\geq 90\%$ down the length of the pore, with minimum at the center of the pore. The pore approaches gas filled, which allows substantial condensation so the equilibrium weight fraction is also substantial.

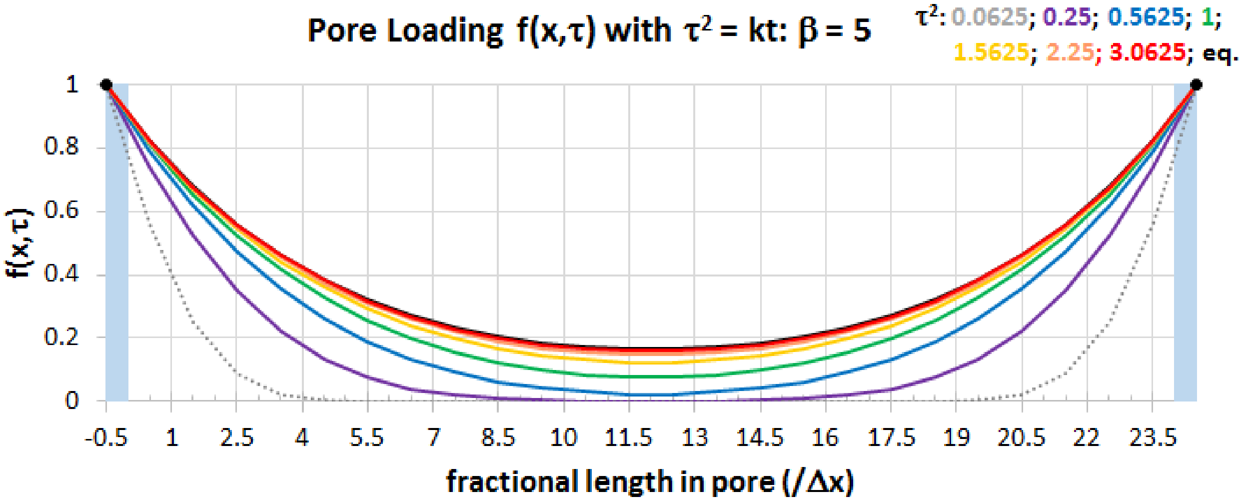

Figure SI.6: For $\beta = 5$, the concentration down the length of the pore increases as a function of time τ^2 where τ^2 is 0.0625, 0.25, 0.5625, 1, 1.5625, 3.0625, and equilibrium. For $\beta = 5$, at equilirbrium the pore is filled $\lesssim 16\%$ at the center of the pore. Because of the low gas content in the pores, the weight change will be less than for lower values of β.

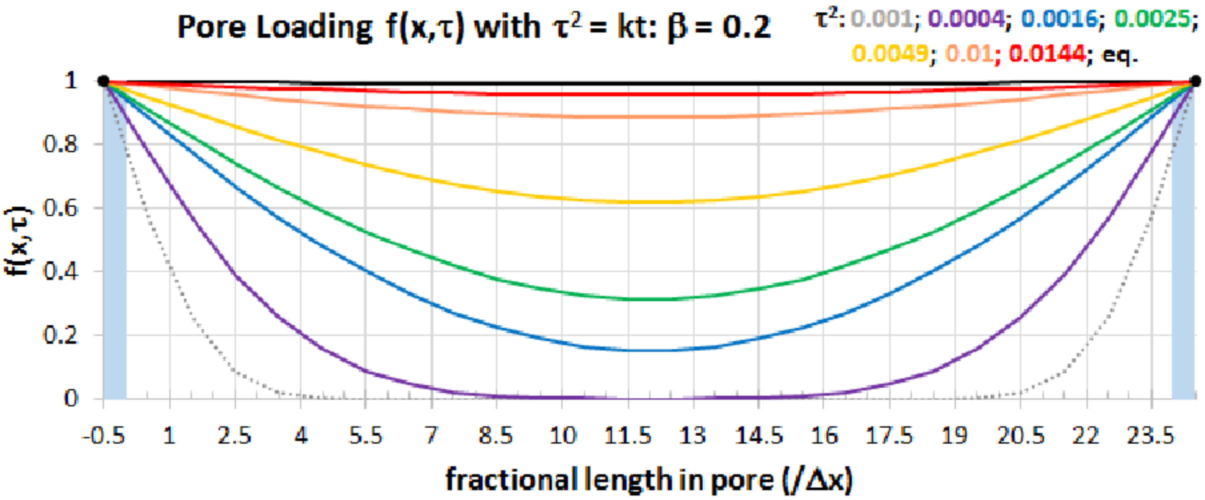

Figure SI.7: For $\beta = 0.2$, the concentration down the length of the pore increases as a function of time τ^2 where τ^2 is 0.001, 0.0004, 0.0016, 0.0025, 0.0049, 0.01, 0.0144, and equilibrium. For $\beta = 0.2$, at equilirbrium the pore is filled $> 99.5\%$ at the center of the pore. The high fraction of gas in the pores allows high degrees of condensation and large weight changes.

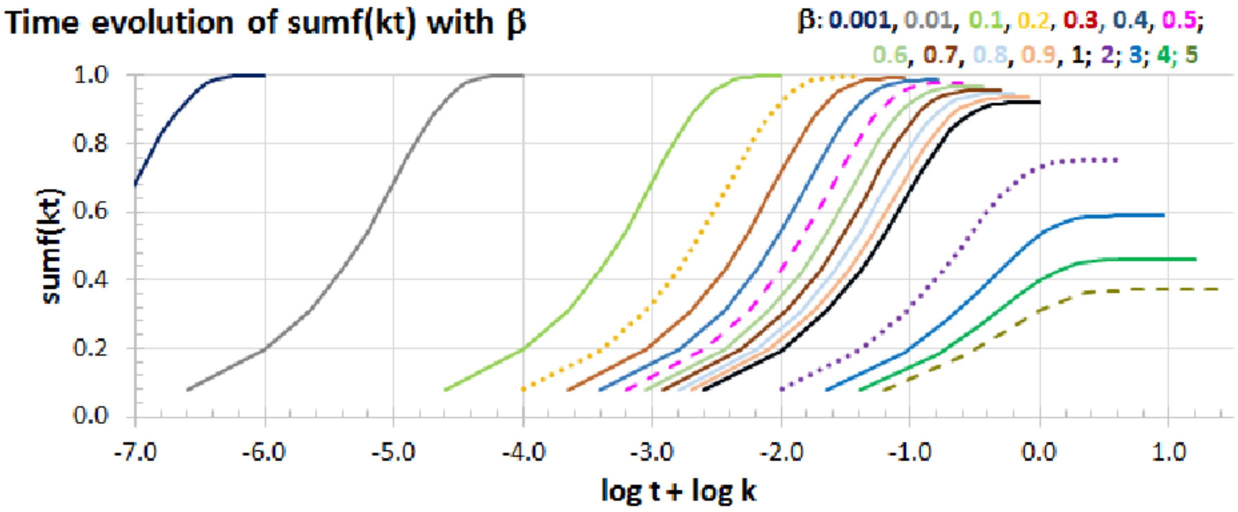

Figure SI.8: The time evolution of $sumf(kt)$ with $\log k + \log t$ for β between 0.001 and 5. For $\beta < 1$, $sumf\,(kt)$ converges to 1 with large shifts on the time axis. For $\beta > 1$, the equilibrium $sumf\,(kt) < 1$. On the plots to aid identifying curves, β of 0.5 and 5 are dashed; β of 0.2 and 2 are dotted. Values are tabulated in Section 8.

mass or density when fully saturated at a given temperature [2]. Here, the calculations are for c^* in g/cm^3. ρ in units of g/m^3

$$RH\,(\%) = 100\frac{\rho}{\rho_{sat}} \tag{SI.52}$$

At 25 °C and 100 % RH, values of 19.96 g H_2O/kg air [3] and 19.673 g/kg [4] or 23.015 g/m^3 are reported. Based on 23.015 g/m^3, .

$$\begin{aligned} c^*\left(g/cm^3\right) &= 0.010 \times RH\,(\%) \times \rho_{sat} \times \left(\frac{m}{100cm}\right)^3 \qquad \text{(SI.53)} \\ &= 10^{-8} RH\,(\%) \times \rho_{sat} \\ &= 10^{-8}\,(23.015) \times RH\,(\%) \\ c^*\left(g/cm^3\right) &= 2.3015 \times 10^{-7} RH\,(\%) \qquad \text{(SI.54)} \end{aligned}$$

For the $RH\,(\%)$ values used in the experiments reported here are shown in Table 1.

Table SI.1: Table of c^* in g/cm^3 for Relative Humidities in Experimental Studies

$RH\,(\%)$	$c^*\left(g/cm^3\right)$
30	6.9045$\times 10^{-6}$
45	10.357$\times 10^{-6}$
60	13.809$\times 10^{-6}$
80	18.412$\times 10^{-6}$
100	23.015$\times 10^{-6}$

2. When data approaches equilibrium, $w_{eq} = 2\pi r \ell^2 N c^* \frac{2}{\beta} \tanh\left[\frac{\beta}{2}\right]$, as expressed in Equation 46 Values of ℓ, r, and N are needed. Alternatively, the porosity ε of particles with straight pores is expressed as volume per gram of sample (cm^3/g), $\varepsilon = \pi r^2 \ell N$. If ε is known, Equation 46 is equivalently expressed as $w_{eq} = 2\varepsilon \frac{\ell}{r} c^* \frac{2}{\beta} \tanh\left[\frac{\beta}{2}\right]$.

   Here, ℓ is taken as the mode of the particle diameters as measured from microscopy images. Images were processed with ImageJ software39 to measure the length of the crystallites. From measurements on 212 particles that were ground before microscopy and sorption experiments, the mode was highest for 2 μm particles, the value for 18% of the particles. The distribution is shown in Figure .9 for the 212 particles examined.

   The radius of the pores was determined by single crystal X-ray diffraction and found to be 6×10^{-8} cm.

   This radius corresponds to channels that are roughly 4 water molecules wide.

   (c) The porosity $\varepsilon = 0.9732$ as determined by
   Given ε, r, and ℓ, N is determined $N = \varepsilon\ \ \pi r^2 \ell^{-\ \ 1} = 4._3 \times 10^{17}$ pores per $\frac{0.9732}{\pi(6\times10^{-8})^2(2\times10^{-4})} =$
   gram of sample.

   (d) The density of the particles is 2.084 g/cm^3

3. For comparison, diffusion coefficients are roughly 0.1 cm^2/s in gases (water in air $D = 0.260$ cm^2/s [5]), small molecules (gases) in water on the order of 1 to several $\times 10^{-5}$ cm^2/s [5].

6.2 Protocol to Fit Experimental Data

Given values of ℓ, r, and either ε or N and an experimentally determined equilibrium weight fraction w_{eq} (mass of water sorbed per mass of particles), data are fit as follows. Start with the equilibrium weight fraction w_{eq}.

1. From the equilibrium data:

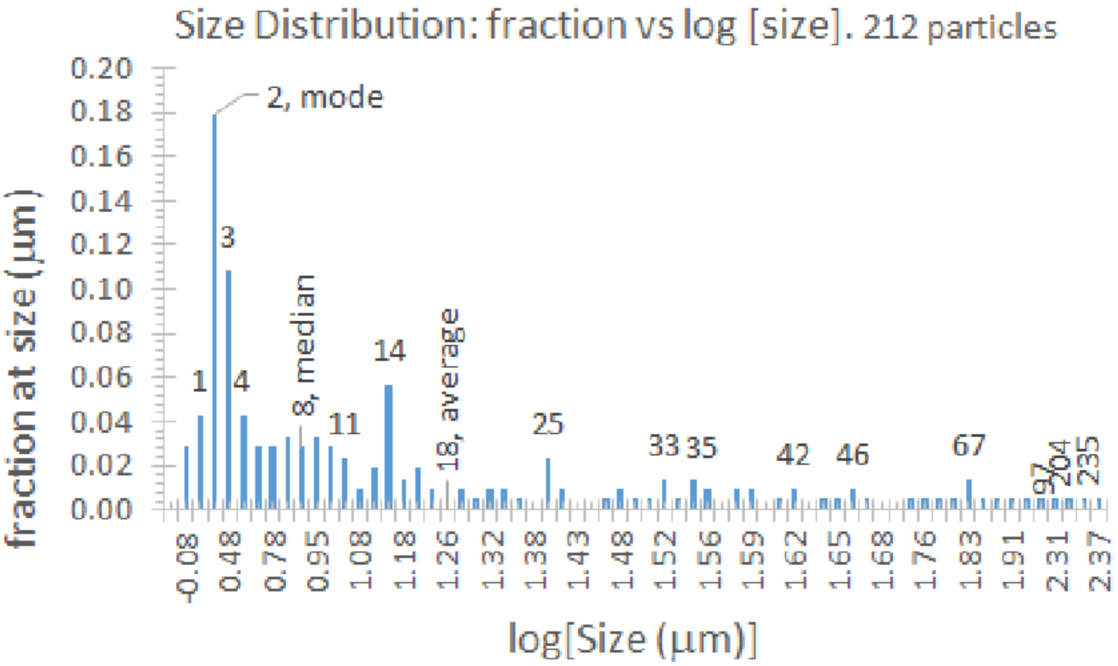

Figure SI.9: The diameters of particles used in the sorption experiments were extracted from microscopy images. In the fitting of the data, ℓ is taken as the mode of the diameter, 2 μm, that accounted for 18% of the particles.

   (a) Calculate the dimensionless value $w_{eq}/\left[2\pi r\ell^2 Nc^*\right]$ or $w_{eq}/\left[2\varepsilon\frac{\ell}{r}c^*\right]$; both expressions are equivalent to $\frac{2}{\beta}\tanh\left[\frac{\beta}{2}\right]$

   (b) Successively estimate β, until the value of β is found such that $w_{eq}/2\pi r\ell^2 Nc^* = \frac{2}{\beta}\tanh\left[\frac{\beta}{2}\right]$ equals $w_{eq}/\left[2\pi r\ell^2 Nc^*\right]$ which equals $w_{eq}/\left[2\varepsilon\frac{\ell}{r}c^*\right]$.
      i. A spreadsheet is a facile means to make the estimates of β.
      ii. An estimate can also be made from Figure .4.

   (c) If data are available for replicates and / or multiple c^* (relative humidities), fit each datum separately. Average the equilibrium values for the replicates after β is found for each datum.

   (d) Generally, given the reproducibility of experimental data, β can likely be estimated with significance to one or two significant figures.

2. From the time dependent data is fit as follows. The spreadsheet and experimental data will have the same maximum, equilibrium value, but the time axes will be offset by $\log k$. Determining the displacement between the fit and the experiment will yield $\log k$.

   (a) Given β and $w_{eq}/2\pi r\ell^2 Nc^*$, use either use a spreadsheet to calculate $sumf\left(\tau^2\right)$ across a range of $\log\left(\tau^2\right)$ for the given β or use the set of tabulated time dependent $w\left(t\right)$ values given in Section 8 or use the Figure as the base. Make a plot of the spread sheet values of $w\left(t\right)/\left[2\pi r\ell^2 Nc^*\right] = w\left(t\right)/\left[2\varepsilon\frac{\ell}{r}c^*\right]$ versus $\log k + \log t$ for the appropriate β.

   (b) Similarly, plot the experimental data as $w\left(t\right)/\left[2\pi r\ell^2 Nc^*\right] = w\left(t\right)/\left[2\varepsilon\frac{\ell}{r}c^*\right]$ versus $\log t$ over the experimentally accessible range.

   (c) If the β for the spreadsheet is correctly chosen, both the model and experimental data will converge to the same value at long times where equilibrium is reached.

   (d) To the x-axis for the spreadsheet data, add $-\log k$ until the experimental and model curves superimpose. Successively approximate value of $k \geq 0$ to find the overlap and k.
      i. It is best to fit the limiting $w_{eq}/\left[2\pi r\ell^2 Nc^*\right]$ and one or more points on the rising portion of $w\left(t\right)/\left[2\pi r\ell^2 Nc^*\right]$. Fit of $w\left(t\right)/\left[2\pi r\ell^2 Nc^*\right]$ roughly between initial and $w_{eq}/\left[2\pi r\ell^2 Nc^*\right]$ is best.
      ii. A spreadsheet is an efficient means to estimate k.

   (e) From the time dependent data, k is determined.

3. From equilibrium data, β is found. If time dependent data are fit, k is found.

   (a) Given $\beta = \ell\sqrt{k/D}$ and k, $\beta^2/k = \ell^2/D$.

   (b) Given ℓ, D is found as $D = k\left[\ell/\beta\right]^2$. From D, the matrix (gas, liquid, clathrate, solid) in the pore can be considered.

6.2.1 Additional Notes

1. Even without time dependent data $w\left(t\right)$, $\beta = \ell\sqrt{k/D}$ can be determined from w_{eq} and either $\pi r\ell^2 Nc^*$ or $\varepsilon\frac{\ell}{r}c^*$.

2. Equation 46 ($w_{eq} = 2\pi r\ell^2 Nc^*\frac{2}{\beta}\tanh\left[\frac{\beta}{2}\right]$ or equivalently $w_{eq} = 2\varepsilon\frac{\ell}{r}c^*\frac{2}{\beta}\tanh\left[\frac{\beta}{2}\right]$) can be simplified in the limits of large and small β.

   (a) $\lim_{\beta\longrightarrow 0}\frac{2}{\beta}\tanh\left[\frac{\beta}{2}\right] \longrightarrow 1$ and $w_{eq} \longrightarrow 2\pi r\ell^2 Nc^*$. From Figure .4 and common mathematical approximations, this is appropriate for $\beta \lesssim 0.25$.

   (b) $\lim_{\beta\longrightarrow\infty}\frac{2}{\beta}\tanh\left[\frac{\beta}{2}\right] \longrightarrow \frac{2}{\beta}$ and $w_{eq} \longrightarrow 4\pi r\ell^2 Nc^*/\beta = 4\pi r\ell Nc^*\sqrt{D/k}$. From common mathematical approximations, this is appropriate for $\beta > 5$.

7 Fit of the Experimental Data

Data were collected for water at 80, 60, 45, and 30% RH. All except 30% RH, exhibit clear increase in $w\,(t)$ with time. The 80, 60 and 30 % RH were recorded for 90 minutes, except in one case of 60% where 105 minutes were collected. For 45% RH, data were collected for 180, 300, and 360 minutes. Data for 80 and 60% were fit to an equilibrium weight at 90 minutes. For 45% data were fit to an equilibrium weight at 90 and at 180 minutes. All fits were made for β of 3 or 4 and $\log k$ of -3.3 to -3.95, which is a good fit. Each fit was for 3 trials.

Data are fit as $\ell = 2 \times 10^{-4}$ cm; $r = 6 \times 10^{-8}$ cm; $\varepsilon = 0.9732$ cm^3/g. Values of c^* are calculated from the relative humidity, as tabulated in Table 1.

7.1 Fit of 80% RH Data

The 3 trials for 80%RH are in good agreement as shown by blue markers in Figure .10, where $w\,(t)\,[2c^*\varepsilon\ell/r]^{-1}$ is plotted against $\log t$.. For each trial, the equilibrium weight w_{eq} was taken as $w\,(t)$ at 90 minutes, which allows estimation of β based on Equation 46 ($w_{eq}/\left[2\pi r\ell^2 Nc^*\right] = w_{eq}/\left[2\varepsilon\frac{\ell}{r}c^*\right] = \frac{2}{\beta}\tanh\left[\frac{\beta}{2}\right]$). The estimates are shown in Table 2.

The 80% RH data are fit by $\beta = 4$ and $\log k = -3.3$. Then, the first order rate of condensation is 5×10^{-4}/s. For $\ell = 2 \times 10^{-4}$ cm, this yields $D = 1.3 \times 10^{-12}$ cm^2/s. This diffusion coefficient is about 100 faster than the self diffusion coefficient for water in ice, but 6 to 7 of orders of magnitude lower than diffusion in liquid water.

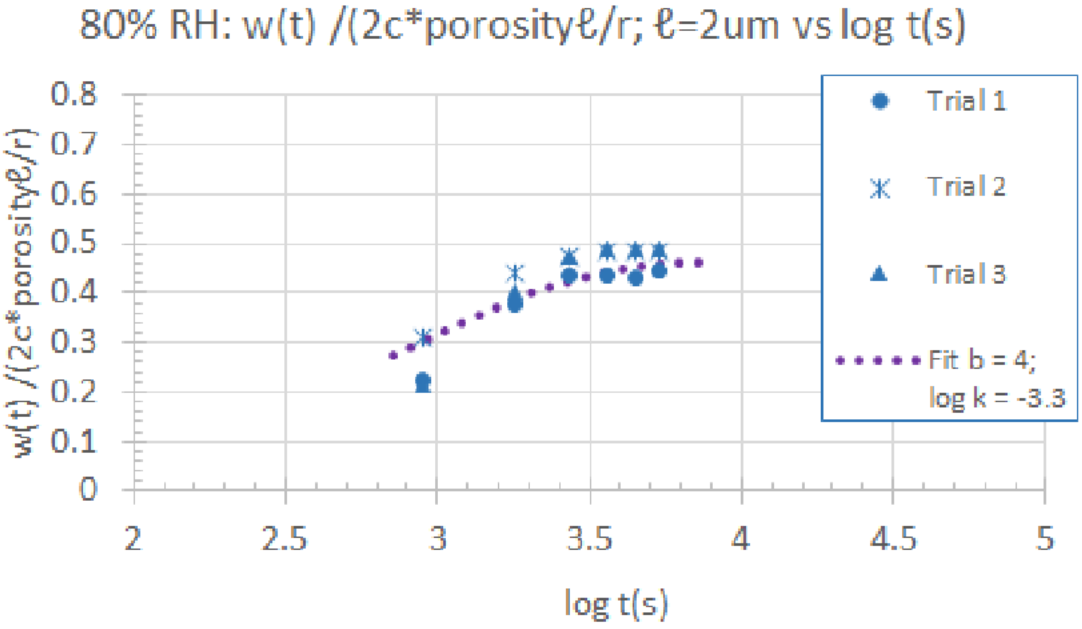

Figure SI.10: Three trials at 80% RH are shown. The equilibrium weights were taken as the values at 90 minutes. The dotted purple line is the fit of the model for $\beta = 4$ and $\log k = -3.3$.

7.2 Fit of 60% RH Data

Two of the 3 trials for 60%RH are in good agreement as shown by green markers in Figure .11, where $w\,(t)\,[2c^*\varepsilon\ell/r]^{-1}$ is plotted against $\log t$.. Trial 2 lags the other two trials but comes to the same equilibrium weight by 90 minutes. For each trial, the equilibrium weight w_{eq} was taken as $w\,(t)$ at 90 minutes and β estimated from Equation 46 ($w_{eq}/\left[2\pi r\ell^2 Nc^*\right] = w_{eq}/\left[2\varepsilon\frac{\ell}{r}c^*\right] = \frac{2}{\beta}\tanh\left[\frac{\beta}{2}\right]$). The estimates are shown in Table 3.

Table SI.2: Fit of 80 % RH Data by Estimation of b.

Trial	$w_{eq}/\left[2\varepsilon\frac{\ell}{r}c^*\right]^{(a)}$	β	$\frac{2}{\beta}\tanh\left[\frac{\beta}{2}\right]$
1	0.445	4.38	0.445
2	0.483	3.99	0.483
3	0.490	3.92	0.490
	average	4.1 ± 0.2	
	For $\beta = 4$		
	$\log k = -3.43$	$k = 5 \times 10^{-4}/s$	
	$\ell = 2 \times 10^{-4}$ cm	$D = 1.3 \times 10^{-12}$ cm^2/s	

(a) Taken from $w\,(3400\ s)$;

The 60% RH data are fit by $\beta = 3$ and $\log k = -3.4$. Then, the first order rate of condensation is 4×10^{-4}/s. For $\ell = 2 \times 10^{-4}$ cm, this yields $D = 1.7 \times 10^{-12}$ cm^2/s.

The values that fit the data for 80 and 60% RH are in excellent agreement.

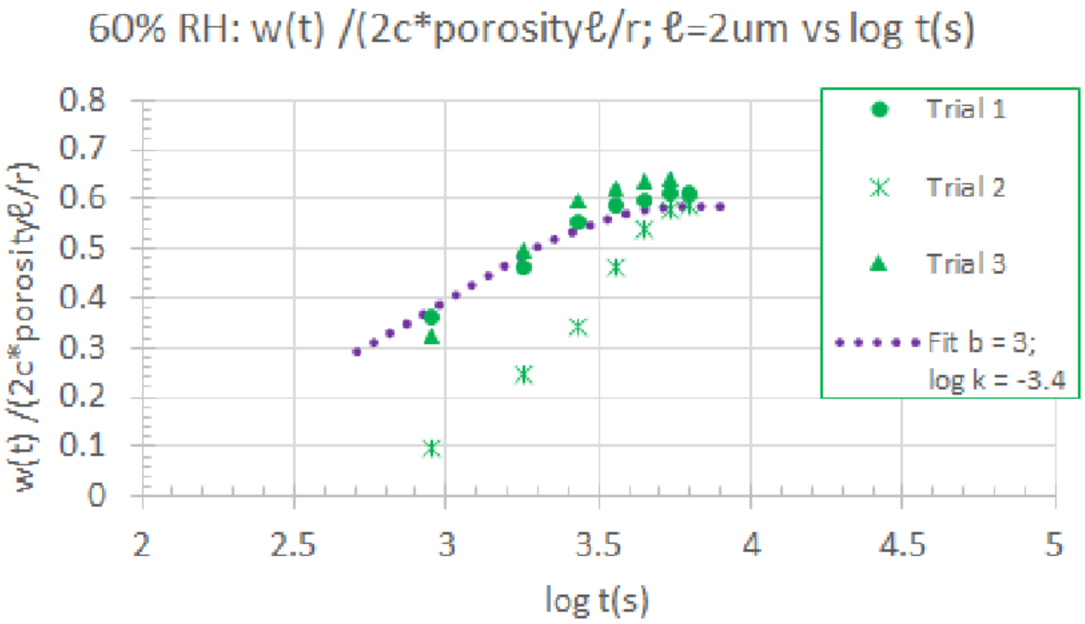

Figure SI.11: Three trials at 60% RH are shown. The equilibrium weights were taken as the values at 90 minutes. The dotted purple line is the fit of the model for $\beta = 3$ and $\log k = -3.4$.

7.3 Fit of 45% RH Data

The 3 trials for 45%RH are in acceptable agreement as shown by red markers in Figure .12, where $w\,(t)\,[2c^*\varepsilon\ell/r]^{-1}$ is plotted against $\log t$.. The three trials are of similar magnitudes with time, but there is variation in the measurement time that allows different estimates of the equilibrium weight. The data are fit to equilibrium weight measured at 90 minutes. But a good fit is also observed for equilibrium measured at approximately 3 hours. For each trial and the equilibrium weight w_{eq} was taken as $w\,(t)$ at 90 minutes, β is estimated from Equation 46 ($w_{eq}/\left[2\pi r\ell^2 N c^*\right] =$

Table SI.3: Fit of 60 % RH Data by Estimation of b.

Trial	$w_{eq}/\left[2\varepsilon\frac{\ell}{r}c^*\right]^{(a)}$	β	$\frac{2}{\beta}\tanh\left[\frac{\beta}{2}\right]$
1	0.610	2.954	0.610
2	0.638	2.76	0.638
3	0.608	2.968	0.608
	average	3.0 ± 0.1	
	For $\beta = 3$		
	$\log k = -3.4$	$k = 4 \times 10^{-4}/s$	
	$\ell = 2 \times 10^{-4}$ cm	$D = 1.7 \times 10^{-12}$ cm^2/s	

(a) Taken from $w\,(3400\ s)$;

$w_{eq}/\left[2\varepsilon\frac{\ell}{r}c^*\right] = \frac{2}{\beta}\tanh\left[\frac{\beta}{2}\right]$).

The 45% RH data where equilibrium weight is taken at 90 minutes are fit by $\beta = 4$ and $\log k = -3.7$. The estimates are shown in Table 4. The first order rate of condensation is 2×10^{-4}/s. For $\ell = 2 \times 10^{-4}$ cm, this yields $D = 5 \times 10^{-13}$ cm^2/s.

The 45% RH data were also fit for equilibrium weight around 180 minutes. This fit is shown as the blue dashed line in Figure .12 for $\beta = 3$ and $\log k = -3.95$. The first order rate of condensation is 1×10^{-4}/s. For $\ell = 2 \times 10^{-4}$ cm, this yields $D = 4 \times 10^{-13}$ cm^2/s. This fit for equilibrium taken at $\sim$ 180 minutes is in good agreement with the fit of the 45% RH where equilibrium is taken at 90 minutes. From these fits in the general range of equilibration times, the model is fairly robust and not critically sensitive to the value of β and $\log k$.

Across the relative humidities of 45 to 80%, the values that fit the data are in very good agreement, well within an order of magnitude.

Table SI.4: Fit of 45 % RH Data by Estimation of b where equilbrium is taken at 90 minutes.

Trial	$w_{eq}/\left[2\varepsilon\frac{\ell}{r}c^*\right]^{(a)}$	β	$\frac{2}{\beta}\tanh\left[\frac{\beta}{2}\right]$
1	0.494	3.89	0.494
2	0.473	4.088	0.473
3	0.453	4.3	0.453
	average	$4.1 \pm$ 0.2	
	For $\beta = 4$		
	$\log k = -3.7$	$k = 2 \times 10^{-4}/s$	
	$\ell = 2 \times 10^{-4}$ cm	$D = 5 \times 10^{-13}$ cm^2/s	

(a) Taken from $w\,(3400\ s)$;

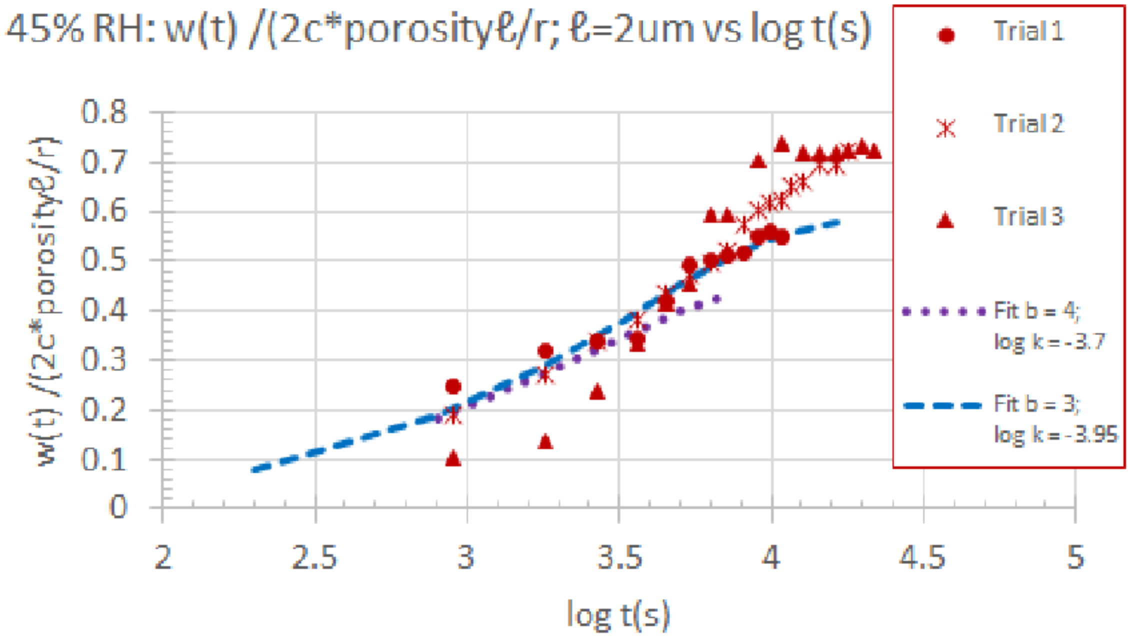

Figure SI.12: Three trials at 45% RH are shown. For equilibrium weights taken at 90 minutes, the dotted purple line is the fit of the model for $\beta = 4$ and $\log k = -3.7$. For equilibrium estimated as closer to the weight at 180 minutes, the data are better fit by $\beta = 3$ and $\log k = -3.95$, as shown by the blue dashed line.

7.4 30% RH Data

Four trials of data were collected at 30% RH for 90 minutes. The data did not approach equilibrium and exhibited significant variability. These data were not fit. Perhaps measurement at longer times may allow a better approach to equilibrium. The weight may be at the limit of detection for these measurements.

The data are shown in Figure for completeness.

8 Tabulated Time Dependent $w\left(t\right)/\left[2\pi r\ell^{2}Nc^{*}\right] = w\left(t\right)/\left[2\varepsilon\frac{\ell}{r}c^{*}\right]$ with $\log\tau^{2} = \log k + \log t$ for Selected β

Spreadsheet values for the time evolution of $w\left(t\right)/\left[2\pi r\ell^{2}Nc^{*}\right] = w\left(t\right)/\left[2\varepsilon\frac{\ell}{r}c^{*}\right]$ as a function of $\tau^{2} = kt$ and $\log\tau^{2} = \log k + \log t$ are provided for 0.001 ≤beta ≤ 5.

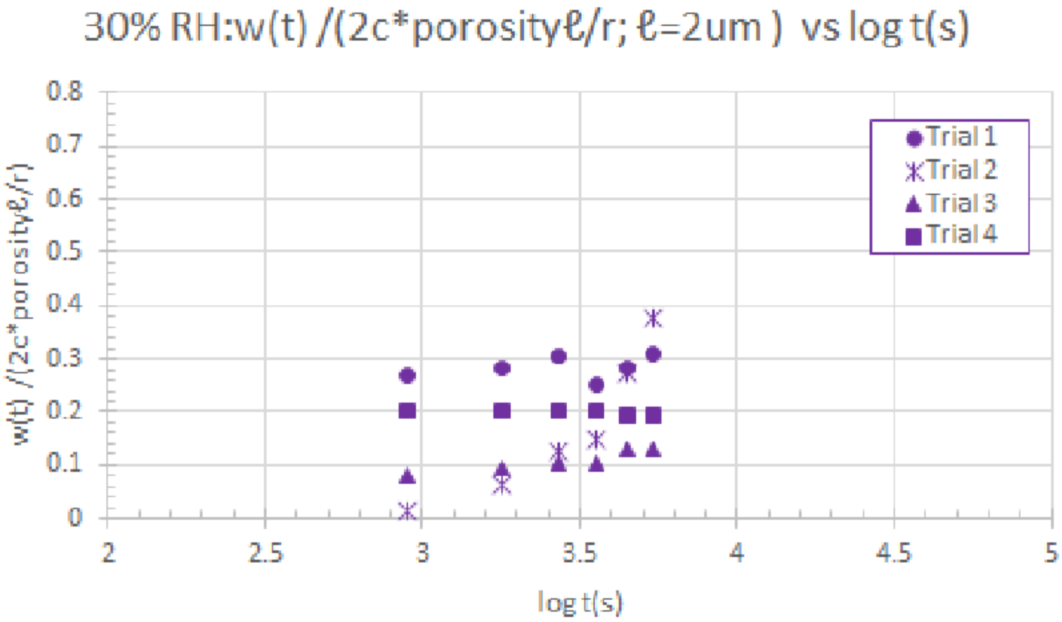

Figure SI.13: Four trials at 30% RH were collected for 90 minutes. Equilibrium is not approached. The data at 30% RH are not fit to the model and are shown for completeness.

	$w(t)/[2\varepsilon(\ell/r)c^*] = w(t)/[2\pi r\ell^2 Nc^*]$				$w(t)/[2\varepsilon(\ell/r)c^*] = w(t)/[2\pi r\ell^2 Nc^*]$				$w(t)/[2\varepsilon(\ell/r)c^*] = w(t)/[2\pi r\ell^2 Nc^*]$		
β		$\tau^2 = kt$	log k + log t	β		$\tau^2 = kt$	log k + log t	β		$\tau^2 = kt$	log k + log t
0.001	0.07902	2.5E-09	-8.602	**0.2**	0.07902	0.0001	-4.000	**0.5**	0.07900	0.000625	-3.204
	0.19498	1E-08	-8.000		0.19495	0.0004	-3.398		0.19479	0.0025	-2.602
	0.31200	2.25E-08	-7.648		0.31189	0.0009	-3.046		0.31134	0.005625	-2.250
	0.42915	4E-08	-7.398		0.42890	0.0016	-2.796		0.42760	0.01	-2.000
	0.54460	6.25E-08	-7.204		0.54411	0.0025	-2.602		0.54159	0.015625	-1.806
	0.65309	9E-08	-7.046		0.65228	0.0036	-2.444		0.64805	0.0225	-1.648
	0.74830	1.23E-07	-6.912		0.74709	0.0049	-2.310		0.74079	0.030625	-1.514
	0.82617	1.6E-07	-6.796		0.82452	0.0064	-2.194		0.81597	0.04	-1.398
	0.88572	2.03E-07	-6.694		0.88365	0.0081	-2.092		0.87291	0.050625	-1.296
	0.92849	2.5E-07	-6.602		0.92603	0.01	-2.000		0.91334	0.0625	-1.204
	0.95741	3.03E-07	-6.519		0.95464	0.0121	-1.917		0.94035	0.075625	-1.121
	0.97585	3.6E-07	-6.444		0.97284	0.0144	-1.842		0.95734	0.09	-1.046
	0.98697	4.23E-07	-6.374		0.98379	0.0169	-1.772		0.96743	0.105625	-0.976
	0.99331	4.9E-07	-6.310		0.99001	0.0196	-1.708		0.97309	0.1225	-0.912
	0.99673	5.63E-07	-6.250		0.99336	0.0225	-1.648		0.97609	0.140625	-0.852
	0.99848	6.4E-07	-6.194		0.99507	0.0256	-1.592		0.97760	0.16	-0.796
	0.99933	7.23E-07	-6.141		0.99589	0.0289	-1.539		0.97831	0.180625	-0.743
	0.99972	**8.1E-07**	**-6.092**		0.99627	0.0324	-1.489		**0.97864**	**0.2025**	**-0.694**
	0.99989	9.03E-07	-6.045		**0.99644**	**0.0361**	**-1.442**		0.97877	0.225625	-0.647
	0.99996	0.000001	-6.000		0.99651	0.04	-1.398		0.97883	0.25	-0.602
0.01	0.07902	2.5E-07	-6.602	**0.3**	0.07902	0.000225	-3.648	**0.6**	0.07899	0.0009	-3.046
	0.19498	0.000001	-6.000		0.19491	0.0009	-3.046		0.19471	0.0036	-2.444
	0.31200	2.25E-06	-5.648		0.31176	0.002025	-2.694		0.31106	0.0081	-2.092
	0.42915	0.000004	-5.398		0.42859	0.0036	-2.444		0.42692	0.0144	-1.842
	0.54460	6.25E-06	-5.204		0.54351	0.005625	-2.250		0.54027	0.0225	-1.648
	0.65309	0.000009	-5.046		0.65127	0.0081	-2.092		0.64585	0.0324	-1.489
	0.74830	1.23E-05	-4.912		0.74558	0.011025	-1.958		0.73752	0.0441	-1.356
	0.82616	0.000016	-4.796		0.82247	0.0144	-1.842		0.81155	0.0576	-1.240
	0.88572	2.03E-05	-4.694		0.88107	0.018225	-1.739		0.86738	0.0729	-1.137
	0.92848	0.000025	-4.602		0.92298	0.0225	-1.648		0.90683	0.09	-1.046
	0.95740	3.03E-05	-4.519		0.95120	0.027225	-1.565		0.93303	0.1089	-0.963
	0.97584	0.000036	-4.444		0.96910	0.0324	-1.489		0.94942	0.1296	-0.887
	0.98696	4.23E-05	-4.374		0.97984	0.038025	-1.420		0.95909	0.1521	-0.818
	0.99330	0.000049	-4.310		0.98592	0.0441	-1.356		0.96447	0.1764	-0.754
	0.99672	5.63E-05	-4.250		0.98919	0.050625	-1.296		0.96731	0.2025	-0.694
	0.99847	0.000064	-4.194		0.99084	0.0576	-1.240		0.96872	0.2304	-0.638
	0.99932	7.23E-05	-4.141		**0.99164**	**0.065025**	**-1.187**		0.96938	0.2601	-0.585
	0.99971	**0.000081**	**-4.092**		0.99201	0.0729	-1.137		**0.96968**	**0.2916**	**-0.535**
	0.99988	9.03E-05	-4.045		0.99217	0.081225	-1.090		0.96980	0.3249	-0.488
	0.99995	0.0001	-4.000		0.99223	0.09	-1.046		0.96985	0.36	-0.444
0.1	0.07902	0.000025	-4.602	**0.4**	0.07901	0.0004	-3.398	**0.7**	0.07898	0.001225	-2.912
	0.19497	0.0001	-4.000		0.19486	0.0016	-2.796		0.19461	0.0049	-2.310
	0.31197	0.000225	-3.648		0.31158	0.0036	-2.444		0.31072	0.011025	-1.958
	0.42909	0.0004	-3.398		0.42816	0.0064	-2.194		0.42612	0.0196	-1.708
	0.54448	0.000625	-3.204		0.54267	0.01	-2.000		0.53872	0.030625	-1.514
	0.65289	0.0009	-3.046		0.64986	0.0144	-1.842		0.64327	0.0441	-1.356
	0.74800	0.001225	-2.912		0.74348	0.0196	-1.708		0.73370	0.060025	-1.222
	0.82575	0.0016	-2.796		0.81961	0.0256	-1.592		0.80639	0.0784	-1.106
	0.88520	0.002025	-2.694		0.87748	0.0324	-1.489		0.86093	0.099225	-1.003
	0.92787	0.0025	-2.602		0.91874	0.04	-1.398		0.89924	0.1225	-0.912
	0.95671	0.003025	-2.519		0.94642	0.0484	-1.315		0.92453	0.148225	-0.829
	0.97510	0.0036	-2.444		0.96392	0.0576	-1.240		0.94023	0.1764	-0.754
	0.98617	0.004225	-2.374		0.97437	0.0676	-1.170		0.94942	0.207025	-0.684
	0.99248	0.0049	-2.310		0.98026	0.0784	-1.106		0.95450	0.2401	-0.620
	0.99588	0.005625	-2.250		0.98341	0.09	-1.046		0.95715	0.275625	-0.560
	0.99762	0.0064	-2.194		0.98500	0.1024	-0.990		0.95846	0.3136	-0.504
	0.99847	0.007225	-2.141		**0.98576**	**0.1156**	**-0.937**		**0.95907**	**0.354025**	**-0.451**
	0.99885	**0.0081**	**-2.092**		0.98611	0.1296	-0.887		0.95933	0.3969	-0.401
	0.99902	0.009025	-2.045		0.98625	0.1444	-0.840		0.95945	0.442225	-0.354
	0.99909	0.01	-2.000		0.98632	0.16	-0.796		0.95949	0.49	-0.310

Figure SI.14: Tabulated Values of $w(t)\,/\,\left[2\pi r\ell^2 Nc^*\right] = w(t)\,/\,\left[2\varepsilon\frac{\ell}{r}c^*\right]$ with $\tau^2 = kt$ and $\log\tau^2 = \log k + \log t$ for $0.001 \le \beta \le 0.7$. For each value, the equilibrium value of $w(t)\,/\,\left[2\pi r\ell^2 Nc^*\right] = w(t)\,/\,\left[2\varepsilon\frac{\ell}{r}c^*\right]$ to three significant figures is marked in bold.

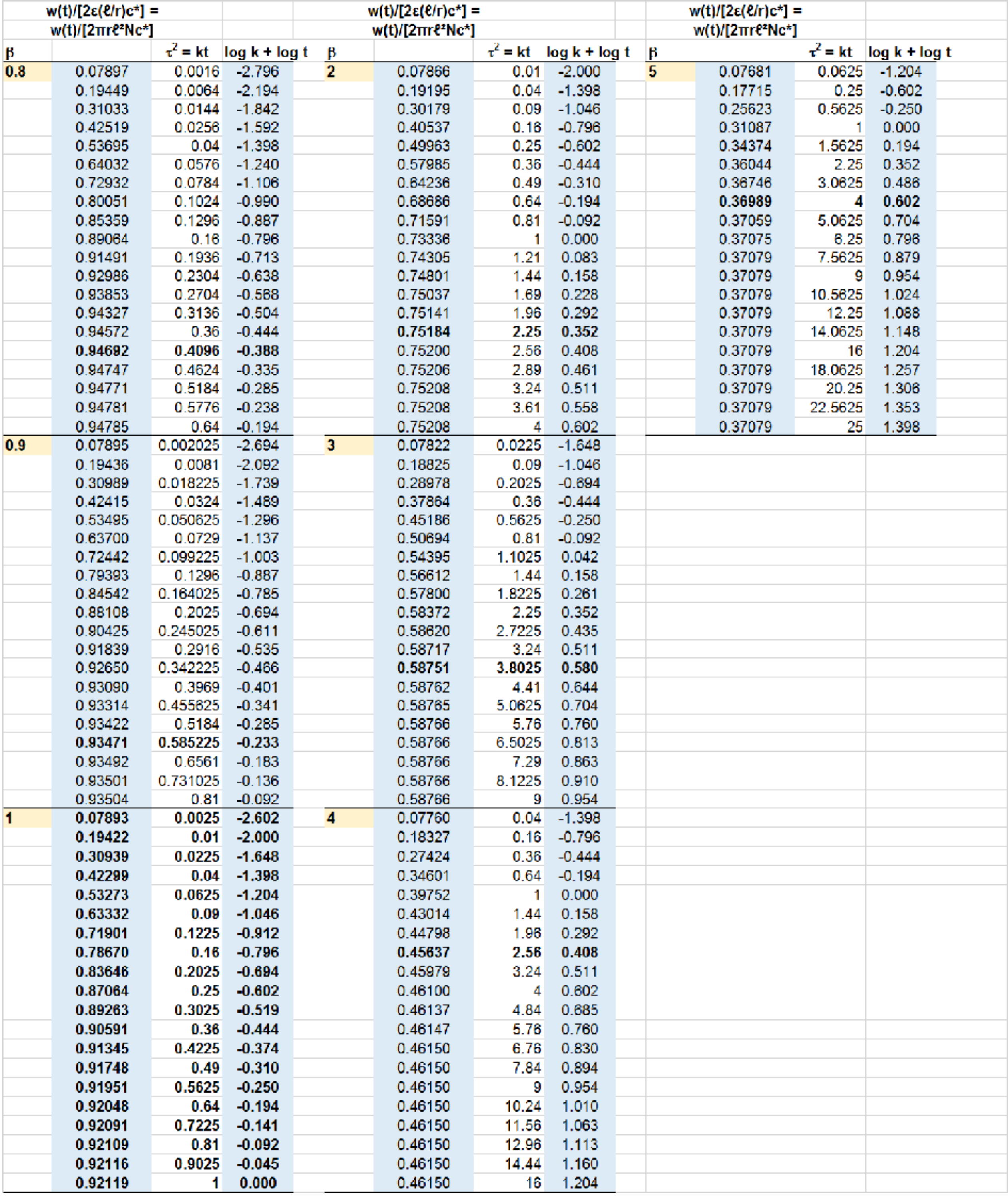

	$w(t)/[2\varepsilon(\ell/r)c^*] = w(t)/[2\pi r\ell^2 Nc^*]$				$w(t)/[2\varepsilon(\ell/r)c^*] = w(t)/[2\pi r\ell^2 Nc^*]$				$w(t)/[2\varepsilon(\ell/r)c^*] = w(t)/[2\pi r\ell^2 Nc^*]$		
β		**τ^2 = kt**	**log k + log t**	**β**		**τ^2 = kt**	**log k + log t**	**β**		**τ^2 = kt**	**log k + log t**
0.8	0.07897	0.0016	-2.796	**2**	0.07866	0.01	-2.000	**5**	0.07681	0.0625	-1.204
	0.19449	0.0064	-2.194		0.19195	0.04	-1.398		0.17715	0.25	-0.602
	0.31033	0.0144	-1.842		0.30179	0.09	-1.046		0.25623	0.5625	-0.250
	0.42519	0.0256	-1.592		0.40537	0.16	-0.796		0.31087	1	0.000
	0.53695	0.04	-1.398		0.49963	0.25	-0.602		0.34374	1.5625	0.194
	0.64032	0.0576	-1.240		0.57985	0.36	-0.444		0.36044	2.25	0.352
	0.72932	0.0784	-1.106		0.64236	0.49	-0.310		0.36746	3.0625	0.486
	0.80051	0.1024	-0.990		0.68686	0.64	-0.194		**0.36989**	**4**	**0.602**
	0.85359	0.1296	-0.887		0.71591	0.81	-0.092		0.37059	5.0625	0.704
	0.89064	0.16	-0.796		0.73336	1	0.000		0.37075	6.25	0.796
	0.91491	0.1936	-0.713		0.74305	1.21	0.083		0.37079	7.5625	0.879
	0.92986	0.2304	-0.638		0.74801	1.44	0.158		0.37079	9	0.954
	0.93853	0.2704	-0.568		0.75037	1.69	0.228		0.37079	10.5625	1.024
	0.94327	0.3136	-0.504		0.75141	1.96	0.292		0.37079	12.25	1.088
	0.94572	0.36	-0.444		**0.75184**	**2.25**	**0.352**		0.37079	14.0625	1.148
	0.94692	**0.4096**	**-0.388**		0.75200	2.56	0.408		0.37079	16	1.204
	0.94747	0.4624	-0.335		0.75206	2.89	0.461		0.37079	18.0625	1.257
	0.94771	0.5184	-0.285		0.75208	3.24	0.511		0.37079	20.25	1.306
	0.94781	0.5776	-0.238		0.75208	3.61	0.558		0.37079	22.5625	1.353
	0.94785	0.64	-0.194		0.75208	4	0.602		0.37079	25	1.398
0.9	0.07895	0.002025	-2.694	**3**	0.07822	0.0225	-1.648				
	0.19436	0.0081	-2.092		0.18825	0.09	-1.046				
	0.30989	0.018225	-1.739		0.28978	0.2025	-0.694				
	0.42415	0.0324	-1.489		0.37864	0.36	-0.444				
	0.53495	0.050625	-1.296		0.45186	0.5625	-0.250				
	0.63700	0.0729	-1.137		0.50694	0.81	-0.092				
	0.72442	0.099225	-1.003		0.54395	1.1025	0.042				
	0.79393	0.1296	-0.887		0.56612	1.44	0.158				
	0.84542	0.164025	-0.785		0.57800	1.8225	0.261				
	0.88108	0.2025	-0.694		0.58372	2.25	0.352				
	0.90425	0.245025	-0.611		0.58620	2.7225	0.435				
	0.91839	0.2916	-0.535		0.58717	3.24	0.511				
	0.92650	0.342225	-0.466		**0.58751**	**3.8025**	**0.580**				
	0.93090	0.3969	-0.401		0.58762	4.41	0.644				
	0.93314	0.455625	-0.341		0.58765	5.0625	0.704				
	0.93422	0.5184	-0.285		0.58766	5.76	0.760				
	0.93471	**0.585225**	**-0.233**		0.58766	6.5025	0.813				
	0.93492	0.6561	-0.183		0.58766	7.29	0.863				
	0.93501	0.731025	-0.136		0.58766	8.1225	0.910				
	0.93504	0.81	-0.092		0.58766	9	0.954				
1	**0.07893**	**0.0025**	**-2.602**	**4**	0.07760	0.04	-1.398				
	0.19422	**0.01**	**-2.000**		0.18327	0.16	-0.796				
	0.30939	**0.0225**	**-1.648**		0.27424	0.36	-0.444				
	0.42299	**0.04**	**-1.398**		0.34601	0.64	-0.194				
	0.53273	**0.0625**	**-1.204**		0.39752	1	0.000				
	0.63332	**0.09**	**-1.046**		0.43014	1.44	0.158				
	0.71901	**0.1225**	**-0.912**		0.44798	1.96	0.292				
	0.78670	**0.16**	**-0.796**		**0.45637**	**2.56**	**0.408**				
	0.83646	**0.2025**	**-0.694**		0.45979	3.24	0.511				
	0.87064	**0.25**	**-0.602**		0.46100	4	0.602				
	0.89263	**0.3025**	**-0.519**		0.46137	4.84	0.685				
	0.90591	**0.36**	**-0.444**		0.46147	5.76	0.760				
	0.91345	**0.4225**	**-0.374**		0.46150	6.76	0.830				
	0.91748	**0.49**	**-0.310**		0.46150	7.84	0.894				
	0.91951	**0.5625**	**-0.250**		0.46150	9	0.954				
	0.92048	**0.64**	**-0.194**		0.46150	10.24	1.010				
	0.92091	**0.7225**	**-0.141**		0.46150	11.56	1.063				
	0.92109	**0.81**	**-0.092**		0.46150	12.96	1.113				
	0.92116	**0.9025**	**-0.045**		0.46150	14.44	1.160				
	0.92119	**1**	**0.000**		0.46150	16	1.204				

Figure SI.15: Tabulated Values of $w(t)\,/\,\left[2\pi r\ell^2 Nc^*\right] = w(t)\,/\,\left[2\varepsilon\frac{\ell}{r}c^*\right]$ with $\tau^2 = kt$ and $\log\tau^2 = \log k + \log t$ for $0.8 \le \beta \le 5$. For each value, the equilibrium value of $w(t)\,/\,\left[2\pi r\ell^2 Nc^*\right] = w(t)\,/\,\left[2\varepsilon\frac{\ell}{r}c^*\right]$ to three significant figures is marked in bold. For $\beta = 1$, all values are marked in bold.

9. Model Fit to MIL-53

1) Extracted the data from the figure and fit the data to the equilibrium model. The experiment is to determine waters per unit cell as function of atmospheric pressure.[6]

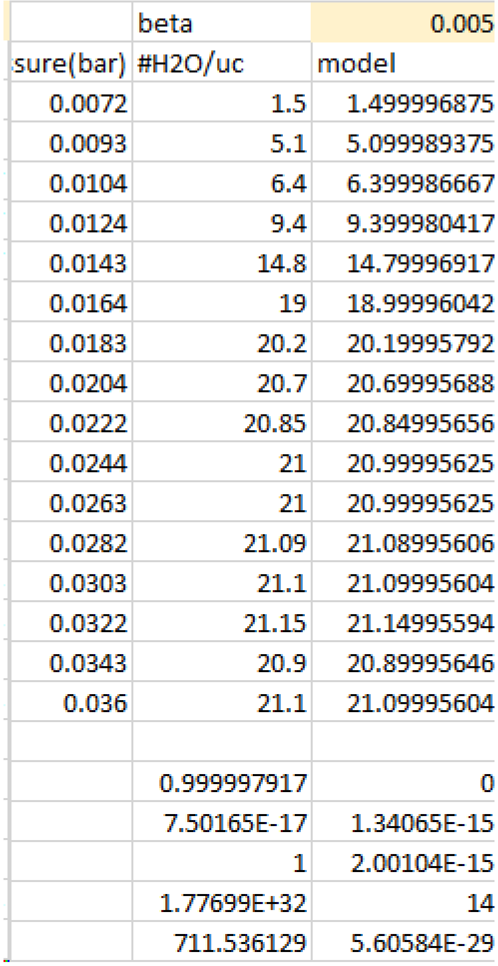

	beta	0.005
sure(bar)	#H2O/uc	model
0.0072	1.5	1.499996875
0.0093	5.1	5.099989375
0.0104	6.4	6.399986667
0.0124	9.4	9.399980417
0.0143	14.8	14.79996917
0.0164	19	18.99996042
0.0183	20.2	20.19995792
0.0204	20.7	20.69995688
0.0222	20.85	20.84995656
0.0244	21	20.99995625
0.0263	21	20.99995625
0.0282	21.09	21.08995606
0.0303	21.1	21.09995604
0.0322	21.15	21.14995594
0.0343	20.9	20.89995646
0.036	21.1	21.09995604
	0.999997917	0
	7.50165E-17	1.34065E-15
	1	2.00104E-15
	1.77699E+32	14
	711.536129	5.60584E-29

Figure SI.16 Extracted water uptake data from MIL-53.

2) The measurements are at equilibrium (not time dependent), so the equilibrium equation applies:

$$w_{eq} = 4\pi r l^2 N c^* \frac{1}{\beta} tanh \frac{\beta}{2}$$

where both sides are dimensionless. The experimental data are fit as shown and tabulated in the table above. In the figure, the blue dot is the experimental data and the red dot is the fit. The correlation for the fit against the experiment is shown and #H_2O/unit cell = (0.999998 +/- 0) P + (0 +/- 1e-15) for **β** = 0.005.

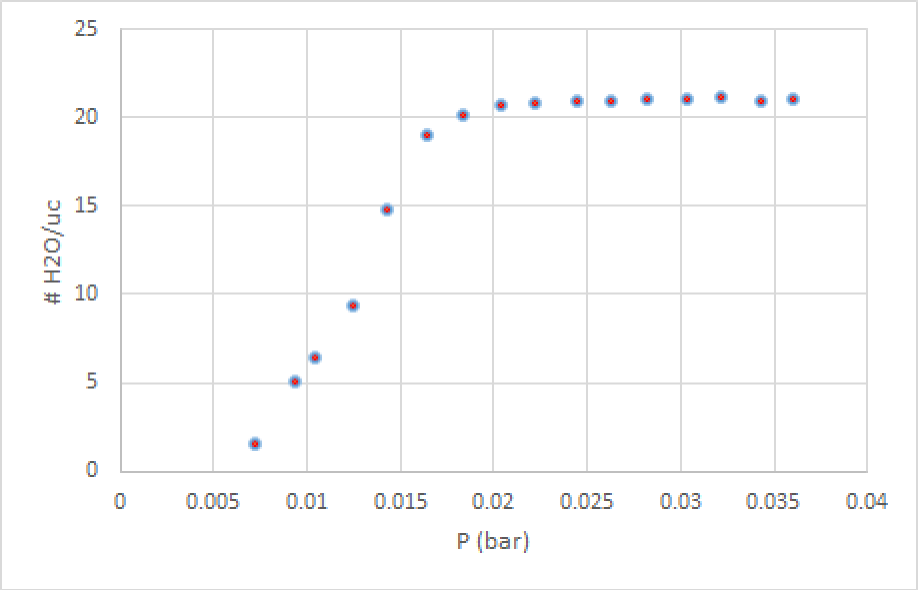

Figure SI.17. Experimental water uptake for MIL-53 (red circles) compared to fit from the model (blue open circles).

3) The fit superimposes for all $\boldsymbol{\beta} < 0.01$. Interestingly, the model even predicts the kink in the curve at about 0.013 bar. Above 0.02 bar, no more water fits in the pore, even if the pressure increases.
4) For any $\boldsymbol{\beta} < 0.25$ (see SI), $\tanh(\boldsymbol{\beta}/2) \rightarrow \boldsymbol{\beta}/2$ and the adsorption curve (as above) is independent of the value of $\boldsymbol{\beta}$, where $\boldsymbol{\beta} = l[k/D]^{0.5}$. For small $\boldsymbol{\beta}$, diffusion is sufficiently fast that no kinetic step limits the response and pore loading is diffusion controlled (no significant kinetic inhibition).

Given the large pores in MIL-53, this makes sense as the water molecules have sufficient space to move around and pack into the pores without kinetic impact. This contrast with the UMON pores described in the paper where the radius of the pores is very small. That is all consistent with the MIL-53 pores being very different from the UMON pores. Unfortunately we were not able to predict a diffusion coefficient for MIL-53 because the data are equilibrium. If the time dependent absorption is reported or the time to equilibrium is known, then a diffusion coefficient might be estimated. It is at least known that $\boldsymbol{\beta} = l[k/D]^{0.5}$ for MIL-53 is smaller than for UMON by about 100 fold and that for MIL-53, there are no significant kinetic steps in the absorption of water.

10. Solvent Vapor Sorption Experiments

10.1 Evolved gas analysis

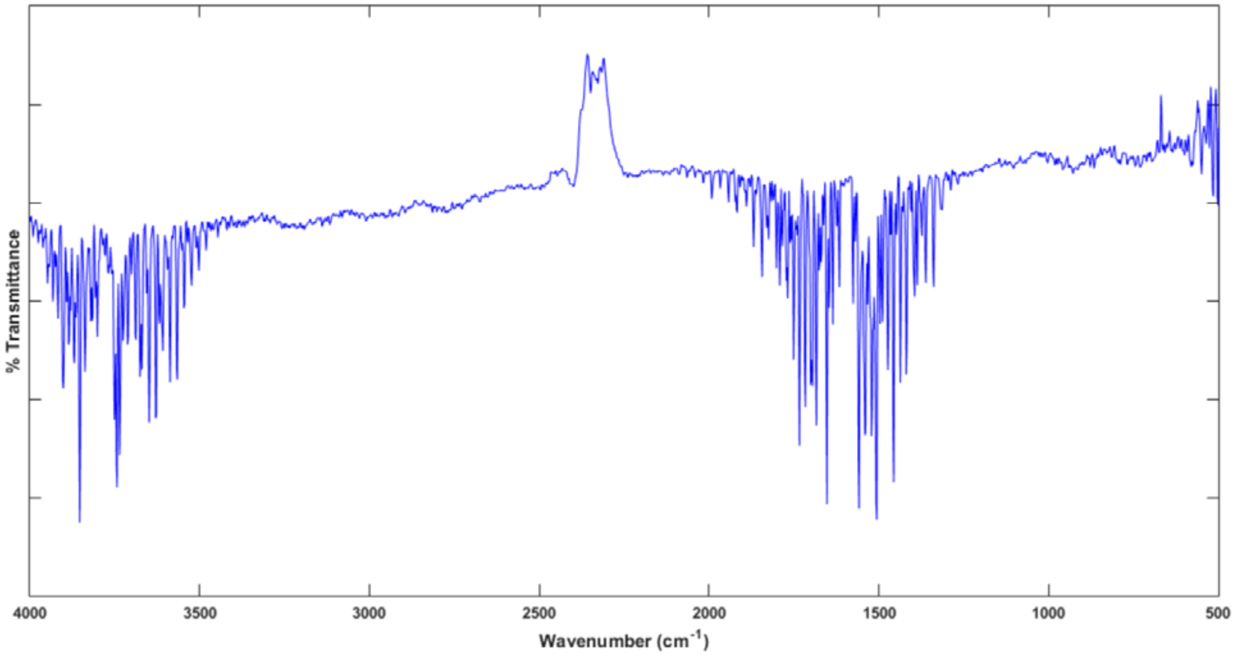

Figure SI.18: Representative FTIR spectra of the vapor phase for gases evolved during the thermogravimetric analysis of UMON exposed to the solvent vapor. Peaks present between 1200-2000 and 3500-4000 cm^{-1} are indicate the presence of gaseous water molecules.

10.2 Degradation of UMON in presence of ammonia vapor

Adsorption of ammonia vapor was also explored because of the potential for hydrogen bonding, but exposure to the UMON material results in degradation of the crystalline phase. Powder X-ray diffractograms of the polycrystalline UMON sample after exposure to NH_3 vapor indicated that crystals are stable up to 15 minutes exposure to NH_3 vapor, but begin to transform after 30 minutes (Figure SI.17). Additional peaks appear in the diffractogram at 7 and 13 °2θ and continue to increase in intensity after one hour of exposure. A secondary transformation occurs after two hours, where the peak at 7 ° 2θ has disappeared, but multiple peaks appear in the diffractogram that do not match with the original UMON material or any other known phase.

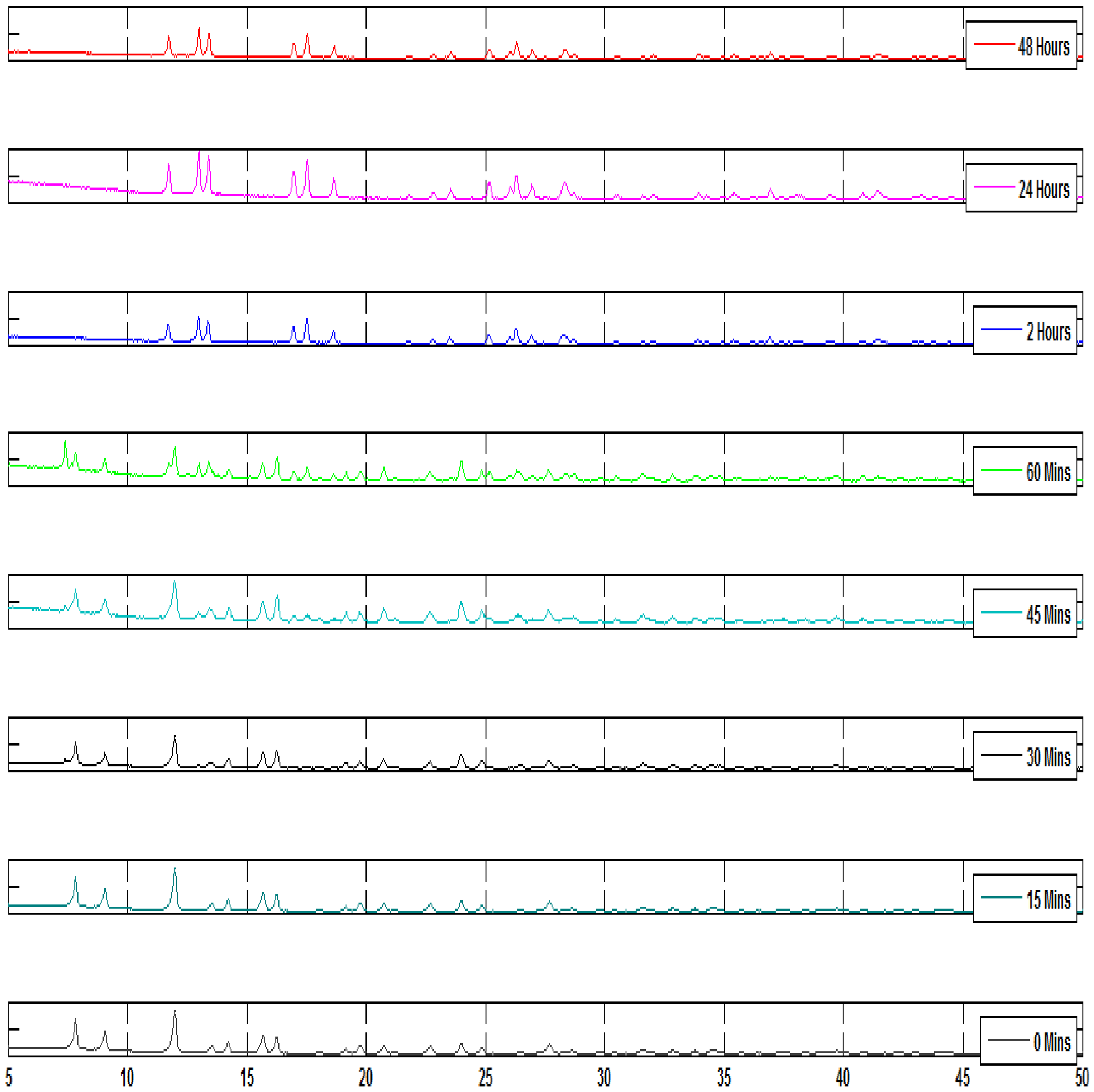

Figure SI.17: Powder X-ray diffractograms were collected of the UMON material after exposure to NH_3 vapor at different time intervals and indicate degradation of starting material.

We previously observed that when UMON crystals were added to NH_3 in methanol dissolution occurred immediately and then quickly precipitated as a secondary phase.[7] This rapid dissolution and re-precipitation resulted in poor crystal quality and the exact structure could not be determined using single crystal X-ray diffraction. We hypothesized that NH_3 disrupts the hydrogen bonding network that stabilizes the 3-D crystalline lattice, resulting in the formation of a secondary phase, but we were unable to confirm the nature of the degradation product. UMON crystals exposed to NH_3 vapor for more than three hours did form crystals that were again not crystalline enough for full analysis by single crystal x-ray diffraction. A partial structure refinement suggests the formation of a 1:2 uranyl iminodiacetate monomer, such as the one previously reported in solution by Jiang et al.[8] The structure may be charge balanced by an ammonium cation, which could be formed by proton abstraction from doubly protonated IDA linker by NH_3 molecule. This in turn could disrupt the hydrogen bonding network of the crystalline lattice and result in a solid state transformation to the degradation phase.

11. References for Supplemental Information Section

[1] G. Doetsch, *Tabellen zur Laplace-Transformation und Anleitung zum Gebrauch*, Springer Verlag, 1947, Berlin and Göttingen, page 109, transform #51.

[2] http://www.engineeringtoolbox.com

[3] http://www.lenntech.com/calculators/humidity/relative-humidity.htm

[4] http://www.cactus2000.de/uk/unit/masshum.shtml

[5] E.L. Cussler, Diffusion Mass Transport in Fluid Systems, 3rd Edition, Cambridge University Press, 2009, Chapter 5.

[6] F. Salles, S. Bourrelly, H. Jobic, T. Devic, V. Guillerm, P. Llewellyn, C. Serre, G. Ferey, G. Maurin, *J. Phys. Chem. C.*, 2011, 115, 10764-10776.

[7] A. S. Jayasinghe, S. Salzman and T. Z. Forbes, *Cryst. Growth & Design*, 2016, **16**, 7058-7066.

[8] J. Jiang, J. C. Renshaw, M. J. Sarsfield, F. R. Livens, D. Collison, J. M. Charnock and H. Eccles, *Inorg. Chem.*, 2003, **42**, 1233-1240.